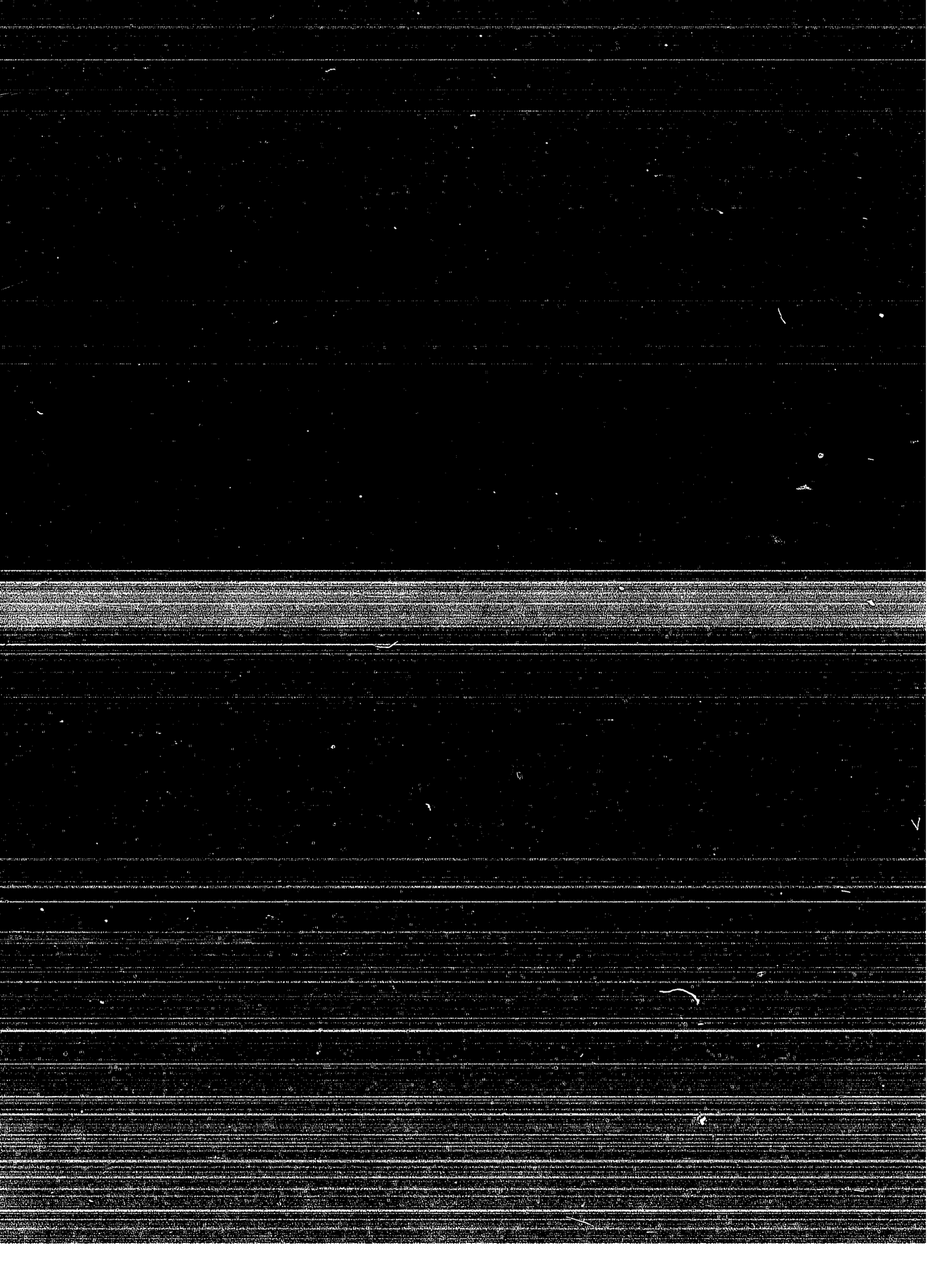

THE UNIVERSITY OF OKLAHOMA

GRADUATE COLLEGE

OPTICAL FREQUENCY DOMAIN REFLECTOMETRY

A DISSERTATION

SUBMITTED TO THE GRADUATE FACULTY

in partial fulfillment of the requirements for the

degree of

DOCTOR OF PHILOSOPHY

BY

MEHDI SHADARAM

Norman, Oklahoma

1984

OPTICAL FREQUENCY DOMAIN REFLECTOMETRY

APPROVED BY

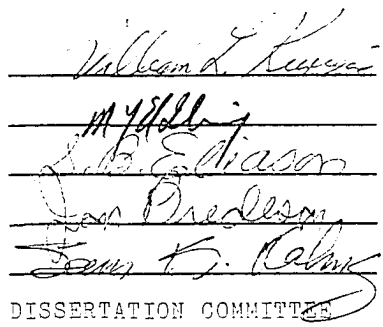

DISSERTATION COMMITTEE

ACKNOWLEDGMENTS

The author wishes to express sincere thanks to Dr. William L. Kuriger for his guidance and supervision throughout the various phases of the graduate study, and acting as the chairman of the dissertation committee.

The author is extremely grateful to the graduate committee members, Dr. Mohamed Y. El-Ibiary, Dr. Seun K. Hahng, Dr. Jon G. Bredeson, and Dr. Stanley B. Eliason for their beneficial suggestions and support.

The author also wishes to acknowledge Miss Rose Brzoska for her assistance in editing various stages of this manuscript.

Finally, the author wishes to express sincere gratitude to his parents for their encouragement and support.

ABSTRACT

The optical frequency domain technique has been used in the analysis of discrete and distributed reflections in an optical fiber. Reflections are studied in three different cases: Discrete reflections only, distributed reflections only, and combination of discrete and distributed reflections. The signal to noise ratio (SNR) for the frequency domain technique has been calculated. A comparative study with the time domain technique has shown an improvement of SNR by an average of 40 dB when frequency domain technique is being used. When discrete and distributed reflections are combined, frequency domain method will be more efficient for detecting discrete reflections. The time domain technique, however, will be a better choice for characterizing the fiber scattering loss and other distributed reflections. Ratio of distributed reflections to the discrete reflections power has been calculated in order to determine the effect of some fiber parameters such as length, backscattering factor S, and scattering loss coefficient α_s on the reflections.

TABLE OF CONTENTS

Table of Contents (Continued)

LIST OF ILLUSTRATIONS

List of Illustrations (Continued)

List of Illustrations (Continued)

List of Illustrations (Continued)

OPTICAL FREQUENCY DOMAIN REFLECTOMETRY

CHAPTER I

INTRODUCTION

Fiber optics is generally regarded as a communications technology for transmitting digital and analog signals. In all fiber optic communication systems there is a need to examine the transmission medium, after it is installed, for fault locations, characterizing the reflecting properties of splices, and for determination of the characteristics of the fiber in a field environment. Optical reflectometry is an effective technique for examination of optical fiber links. When light passes through an optical fiber , it will be reflected back by two mechanisms: Fresnel reflection that occurs as light passes into a medium having a different index of refraction, and Rayleigh scattering which is caused by microscopic variations in the core refractive index. The echos from the front face, splices, or perfect breaks(Fresnel reflections) in a fiber are much higher than Rayleigh reflections. In general there are two methods of optical reflectometries: Optical Time Domain Reflectometry(OTDR) (P1,N1,R1, A1,P2,N2) and Optical Frequency Domain Reflectometry (OFDR) (M1,E1)

1.1 OTDR

In essence, an OTDR is a one dimensional, closed-circuit, optical radar. It operates by periodically launching short duration laser pulses into one end of the fiber under test and monitoring the amplitude and temporal characteristics of the reflected light. Fresnel reflections will appear as a sharp spike in the backscattered signal with a delay, which is in accordance with the reflector location. Rayleigh scattering, which results from distributed reflections, causes a continuous reflected signal of very low amplitude. It is well known that the backscattered power decays exponentially according to the value of Rayleigh scattering coefficient for fibers with uniform structure along the fiber axis. In general, however, the backscattered power does not decay exponentially for fibers with structural parameter fluctuations along the fiber axis. OTDR can, therefore, be used for the attenuation characteristic measurements of optical fibers and splices and for fault location.

1.2 OFDR

The OFDR in this research requires a CW optical carrier which is intensity modulated by a constant amplitude rf signal. A phase and amplitude variation will be introduced to the envelope of the echos, which corresponds with the reflector distance from the transmitter side, Rayleigh scattering loss, core index of refraction, and rf frequency. By changing the rf and observing the phase and amplitude of the reflected

signal's envelope, properties of the fiber can be studied. The sweep technique (M1,K1) can also be used in OFDR. In this method the returned signals are multiplied with the modulation signal to produce a correlation signal in the frequency domain, which is then observed by means of a spectrum analyzer. The noise power of optical receivers is proportional to the receiver bandwidth. In frequency domain reflectometry, the receiver bandwidth is directly proportional to the resolvable distance. Thus the frequency domain SNR improves by comparison with the time domain SNR as the resolution is made finer. Because unlike the frequency domain, in time domain reflectometry the receiver bandwidth is inversely proportional to the resolvable distance.

1.3 Purpose of the Research

The main purpose of this research is focused on the analysis and detection of discrete (Fresnel) and distributed (Rayleigh) reflections in fiber optics using frequency domain technique. The reflected signals are analyzed in three different categories:

(1) The ratio of relative signal strength of Fresnel reflections is much higher than Rayleigh reflections. The particular application of this case is for detection of faults and measuring uniformity and the insertion loss of splices and connectors. In practice however, faults or breaks are unlikely to produce an ideal cleave, and the Fresnel reflec-

tion power will generally fall short of its maximum.

(2) The ratio of the relative signal strength of Rayleigh reflections is much higher than Fresnel reflections. These reflections can be obtained by using a long fiber and immersing the fiber end in index-matching fluid. These types of reflections can provide information about fiber attenuation.

(3) The ratio of the relative signal strength of Fresnel reflections is almost equal to Rayleigh reflections. The situation for this case can be exemplified by cutting the fiber end in an angle, using a long fiber, or bending the fiber. These reflections can be used to determine the microbend reflections or detection of faults at distances exceeding 30 dB (G1) round trip loss.

The organization of this thesis is as follows: In chapter 2, history of optical reflectometry in general, and optical frequency domain reflectometry for our purpose in particular, are discussed.

Theoretical analysis of discrete and distributed reflections are shown in chapter 3. The reflected signals are analyzed for three different cases: (1) discrete reflections only, (2) distributed reflections only, (3) combination of discrete and distributed reflections.

Chapter 4 illustrates the calculated results. The chapter contiues with SNR calculation for OFDR. Also in this chapter, a comparative study with time domain technique

is presented, and advantages/disadvantages of frequency domain technique are discussed.

Chapter 5 explains the different aspects of the OFDR on the basis of the results of the chapter 4. Subjects which are discussed in this chapter are: frequency effects on the returned signals and dependency of distributed discrete reflection ratio to the fiber parameters.

Chapter 6 illustrates the technique and measuring apparatus used for the experimental part of this thesis. A brief description of each unit in the experimental setup is given. The function of each unit in the experimental setup is tested and discussed separately.

Chapter 7 is the conclusion.

CHAPTER II

REVIEW OF LITERATURE

Because optical communication systems have grown in recent years, much attention has been devoted to the investigation and study of reflections and backscatter in optical fibers. Different techniques of reflectometry have been developed.

A major breakthrough of reflectometry was in 1977, when Personick (P1) analysed the backscattered in a multimode fiber. His analysis was based on geometrical optics. He used a GaAs injection laser to produced pulses of light having a high peak power and a narrow width (5 ns in duration) and had incorporated an avalanche photodiode (APD) receiver. The instrument was capable of detecting echos from breaks or imperfections that were 65 dB below the 4-percent echo from a perfect break. The distance resolution was 0.5 m. He has shown that the backscattering signal power present at the beginning of the fiber is given by

$$P(t)=E_0 S\alpha_s\left(\frac{c}{n}\right) \exp\left(-2\alpha\left(\frac{ct}{2n}\right)\right) \qquad (2\text{-}1)$$

where

P(t) is the received backscattered power as a function

of time,

E_0 is the transmitted pulse energy,

S is the portion of the scattered light guided back towards the transmitter,

α_s is the scattering loss (nepers per meter),

c is the speed of light,

n is the core's index of refraction, and

α is the fiber attenuation (neper per meter).

Therefore, the backscattered Rayleigh scattering could be used to estimate the loss as a function of position along the fiber.

Aoyama and Nakagawa (A1) have developed a theoretical and experimental study of an optical time domain reflectometer in a single-mode fiber. Their investigation has been focused on fault location and application of OTDR to loss measurement of a single-mode fiber. They have calculated the backscattered power with Gaussian beam approximation. The SNR has been calculated at 0.85, 1.3, and 1.55 μm. The 1.3 μm optical source wavelength has been the most suitable of three wavelengths. They used a polarization splitter type directional coupler with their 1.3 μm InGaAsP laser and ADP, and detected a fiber break at the end of 17 km of fiber. This polarization-sensitive device caused problems with loss measurements, but provided good isolation from the input Fresnel reflection. The subsequent use of a polarization scrambler allowed splice and attenuation measurements out to 7 km while detecting a break at 17 km.

Heckman (H1) used fibers which were single-mode at 0.82 μm with a conventional CW laser diode operating in the pulsed mode at 0.82 μm. The dynamic range was 12 dB of one-way loss, and attenuation and splice loss measurements were made over 5 km of fiber.

Philen and White (P2) used an Nd:YAG laser which was operating at 1.064 or 1.319 μm as a source. The laser was Q-switched by the use of an acoustooptic modulator operating at 500 Hz to provide pulses of 0.7 μs duration at 1.064 μm, and 1.7 μs at 1.319 μm. Seven reels of different single-mode fibers were spliced together to give a length of 20.4 km with additional fibers spliced to generate a 28.5 km length. Their measurement for one-way loss of the 20.4 km including splices was 22 dB, which was an average loss of 1.08 dB/km. For 28.5 km, the one-way loss 31.3 dB which resulted in an average of 1.1 dB/km. They also considered the power required to generate nonlinear frequency components such as stimulated Raman scattering, which is known as the critical power. They measured the critical power for the onset of nonlinear effects for each wavelength and found it to be 4.4 W at 1.064 μm and 3.6 W at 1.319 μm. Their calculations for critical power showed 4.3 and 3.0 W for 1.064 and 1.319 μm, respectively.

Murakami and Noguchi (M2) have used the stimulated Raman scattering effect to calculate the maximum measurable distance for a single-mode optical fiber fault locator. Their calculations were carried out on the assumption that

the light source be a Q-switched Nd:YAG laser operating at 1.06 μm and the photodiode be a germanium avalanche photodiode. Fiber loss was considered to be the sum of ultraviolet absorption loss, infrared absorption loss, Rayleigh scattering loss, waveguide imperfection loss, and OH absorption loss. As a result, they obtained the following conclusions:

(1) There is an optimum value in the fiber input optical power where, if the fiber is exited with this optimum power, a fault can be located up to 165 km away in an ultra-low loss fiber.

(2) Optimum input power varies with fiber loss and fiber parameters, but the maximum measurable distance is determined by fiber loss at 1.60 μm. The distance decreases as the loss becomes higher.

To increase the dynamic range of a conventional backscattering technique in which a beam splitter and polarizer-analyzer combination are utilized, Nakazawa and Tanifuji (N1) have developed a new backscattering technique in a single-mode optical fiber by using a TeO acoustooptical light deflector at 120 MHz. A conventional system inevitably suffers from a sacrifice of the backscattered power level by 9 dB due to the beam splitter (a roundtrip: 6 dB) and the analyzer (3 dB) because the backscattered signal is polarized. The new technique adopts an acoustooptical light deflector instead of the beam splitter and the polarizer-analyzer combination. Therefore, Nakazawa and Tanifuji

could increase the dynamic range of the backscattered signal by at least 10 dB, which corresponds to the extension of 5 km in measurable length for fiber loss of 1 dB/km.

Shibata and Tateda (S1) have used the backscattering technique for measurements of waveguide structure fluctuation in multimode optical fibers. They have found z-dependent (z is the coordinate along the fiber axis) backscatter coefficient as a function of fiber structural parameters which are: the relative index difference between core and cladding, the core radius, and the exponent of the power law. They have calculated that the error in the structural parameter fluctuation measurement by their technique was far less than that of the direct measurement.

The longitudenal variation of fiber's characteristic parameters has been also investigated by Mickelson and Ericksurd (M3). One result of their theory is a technique for separating loss and parameter fluctuations. They have implemented and applied this mode-filtering technique to the problem of determining the diameter variation along the fiber length. More experimental work is necessary before this technique can be used to determine arbitrary parameter fluctuations such as Rayleigh scattering coefficient, profile parameter, and numerical aperture variation with certainty.

All backscattering techniques mentioned above make use of the information contained in the intensity of the reflected light. However, there are many external influences (magneticfield, electric field, pressure, temperature, etc.)

which act to change the polarization state of the light propagating in the optical fiber. This change of polarization state makes the use of optical fibers as sensors possible. In a multimode step-index or graded-index fiber each individual transverse mode will possess an independent polarization state, thus leading to an output transverse polarization profile which will be complex and difficult to use unless the number of allowable modes is very small. However, in a step-index single-mode fiber the radiation propagates in a single well-defined polarization state; any perturbation of this state brought about by an external influence is thus more easily detected.

Different devices which measure the integrated effect of external fields along a single-mode fiber have been developed (K2,S2,U1,S3,L1). Roger (R1) combined these techniques with those of OTDR and investigated a new technique which allowed determination of field distribution along the length of a single-mode fiber. This new technique is designated as Polarization Optical Time Domain Reflectometry (POTDR). When a narrow pulse of light is launched into a single-mode fiber, it is continuously Rayleigh scattered as it propagates along the fiber. In POTDR, the backscattered light contains polarization information which can be processed to determine the distribution, along the length of the fiber, of a variety of external influences. Some practical applications of POTDR are as follows:

(1) Sources of electromagnetic interference (EMI) in an electrical system can be identified by laying an optical fiber adjacent to the vulnerable electrical conductors of such a system, and using POTDR to measure either the electric or magnetic field distribution.

(2) Faults on extended power transmission or communication systems are very often accompanied by an anomaly in the electric and/or magnetic field distribution. Such faults could be located using POTDR.

(3) Vibrational modes in large structures such as power station boilers or chemical engineering containers are indicative of certain conditions. These vibrations may be monitored by means of POTDR.

(4) It is possible to use the transverse quaratic electrooptic effect (Kerr effect) in conjunction with POTDR for measurement of voltage on power transmission systems.

(5) In some large structures it is very often desirable to monitor the temperature distribution. The POTDR technique would allow such temperature distributions to be monitored.

Neil Ross (R2) has investigated the birefringence measurement in optical fibers by POTDR. He has analyzed the technique of POTDR to see how the polarization properties of

an optical fiber may be deduced from the backscattered light. In this analysis, he has made the following assumptions:

(1) The effect on the polarization of light traveling along the fiber may be described as a system of linear retarders and rotators.

(2) When the light is scattered at some point in the fiber and is trapped in the mode traveling back toward the source, the scattering process does not alter the amplitude and phase relationship between the two orthogonal components of the electric field vector of the polarized component of the light.

(3) If light travels through the fiber in the reverse directions, the linear birefrignece is the same but the direction of rotation of any rotators is reversed.

Neil Ross has also used the Mueller calculus (G2) in order to measure the birefringence from the Stokes parameters.

Reflectometry in the time domain has been extensively investigated as a method of detecting reflections and backscattering in optical fibers. But, there are not many reports on optical frequency domain reflectometry. Mac Donald (M1) has shown that reflectometry in the frequency domain may have certain advantages for the detection of discrete reflections and SNR improvement. He has suggested that frequency domain measurements may thus aid in charac-

terizing the reflecting properties of splices, connectors, couplers, mode converters, microbends, and similar discretely reflecting elements in optical fibers. A correlation reflectometer which is adapted to detecting weak discrete reflections and operating in frequency domain has been introduced by Mac Donald. He has reported the detection of weak end reflections in a 2.2 km length of fiber whose end was index matched. A round trip loss of 70 dB has been also obtained with a 1 mW optical source power.

CHAPTER III

THEORY

This chapter illustrates a theoretical analysis of the OFDR used for this thesis. Calculations are carried out on the assumption that the light source is a He-Ne laser operating at 0.6332 μm and output power of 10 mW. The photo-detector is a silicon PIN diode (Si-PIN). The intensity modulation index is 15 percent and modulation frequency can be varied from 0.35 to 50 MHz. Backscattered signals are studied for three cases: discrete reflections (Fresnel reflections), distributed reflections (Rayleigh reflections), and discrete and distributed reflections together.

3.1 Detection of Discrete Reflections

In this case of discrete reflections, light traveling along an optical fiber will be reflected from different points due to splices, connectors, breaks, microbends, etc.. Figure 3.1 shows a schematic diagram of an optical fiber with differrent reflectors along it. Next, consider a sinusoidally intensity modulated laser light incident on the fiber. The electrooptically modulated input power to the fiber can be

presented as:

$$P_{in}(t)=E_0(1+m\cos\omega t) \qquad (3.1)$$

where

E_0 is He-Ne laser output power,

m is modulation index, and

ω is modulation frequency.

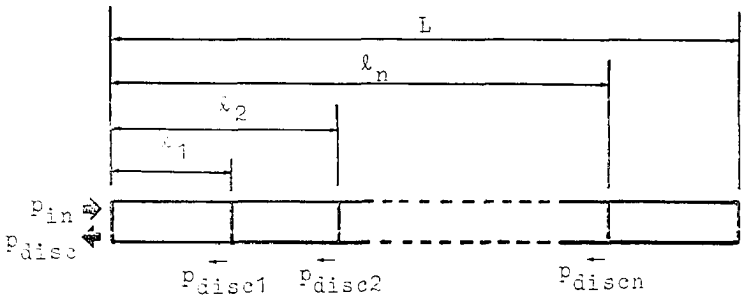

Figure 3.1: Schematic diagram of a fiber optic with discrete reflections

Since the envelope of the reflected signal is employed in the measurements, only the sideband terms are of interest. Therefore, the input optical power at frequency ω will be shown as:

$$P_{in}(t)=p_0\cos\omega t$$

where $p_0=mE_0$ (3.2)

The reflected light power output from the fiber front end can be designated as:

$$p_{disc}=p_{disc1}+p_{disc2}+\cdots+p_{discn} \qquad (3.3)$$

where p_{disci} represents the reflected light power outputted from the ith reflector, and it can be shown as:

$$p_{disc1}=A_1 \cos(\omega t-\theta_1)$$

$$p_{disc2}=A_2 \cos(\omega t-\theta_2)$$

$$\vdots$$

$$p_{discn}=A_n \cos(\omega t-\theta_n).$$

In the above equations A_i and θ_i can be represented as:

$$A_i=p_0(1-T_i)\prod_{k=1}^{i-1} T_k^2$$

$$\theta_i=\frac{2n\omega\ell_i}{c}$$

where

T_i is power transmission coefficient of ith reflector,

ℓ_i is ith reflector distance from the fiber front end,

n is the core index of refraction, and

c is speed of light in free space.

By some mathematical manipulations, p_{disc} can be converted to the form

$$p_{disc}=A_{disc}\cos(\omega t-\theta_{disc}) \qquad (3.5)$$

where A_{disc} and θ_{disc} can be represented as:

$$A_{disc}=\sqrt{\left(\sum_{i=1}^{n} A_i \sin\theta_i\right)^2+\left(\sum_{i=1}^{n} A_i \cos\theta_i\right)^2} \qquad (3.5)$$

$$\theta_{disc}=\text{Arctan}\ \frac{\sum_{i=1}^{n} A_i \sin\theta_i}{\sum_{i=1}^{n} A_i \cos\theta_i} \qquad (3.6)$$

Equations (3.5) and (3.6) show that the amplitude and phase of the reflected power for the discrete reflection case (when Rayleigh reflections are small compared with Fresnel reflections) corresponds with the position and reflectivity of each reflector. Also, it is related to the frequency of modulation. For a given number of reflectors with their positions and reflectivities, and a given frequency, p_{disc} can be represented as a phasor whose length corresponds to the magnitude A_{disc} and whose angle with respect to the positive real axis corresponds to θ_{disc}, as shown in figure 3.2a. Thus a set of values of p_{disc} for values of f (modulation frequency) between 0 and ∞ yields a set of phasors whose tips are connected by a smooth curve, as shown in figure 3.2b. Therefore, for certain reflectors along a fiber, a phasor-locus can be developed for p_{disc} in the complex plane by varying the modulation frequency. The graphical representation of the phasor-locus depends on the reflector's

characteristics.

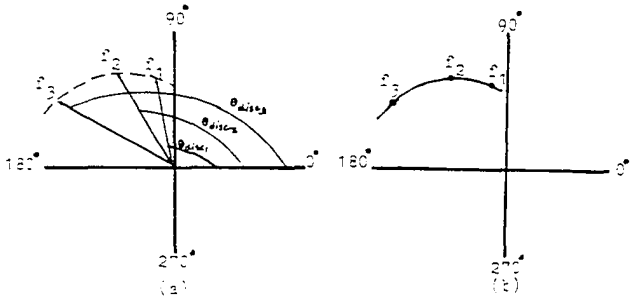

Figure 3.2: Phasor-locus development of p_{disc}

3.2 Detection of Distributed Reflections

In the case of distributed reflections, light traveling along the fiber will be reflected continuosly due to scattered reflections such as Rayleigh scattering. This type of scattering depends on the short range molecular ordering in the fiber medium. Continuous scattering can also be Rayleigh-Mie scattering, either from imperfections or from impurities within the medium. Suppose a sinusoidally intensity modulated light, which has been described in section 3.1, is launched into the fiber shown in figure 3.3. A fraction of light power which enters the element which lies between ℓ and $\ell+d\ell$ along the fiber will be backscattered toward the launch end as a consequence of scattering and absorption processes.

This fraction will be given by

$$p(\ell)=\alpha_s S P_0 \exp(-2\alpha\ell)\ \cos(\omega t-\frac{2\omega\ell n}{c}) \qquad (3.7)$$

where α, α_s, and S are discussed in chapter 2.

Figure 3.3: Schematic diagram of an optical fiber with distributed reflections.

It has been shown that (V1,C1) the recaptured factor S for a step-index multimode fiber is

$$S_{step}=\frac{3(NA)^2}{8\ n_1^2} \qquad (3.8)$$

and that for a graded-index multimode fiber is

$$S_{graded}=\frac{(NA)^2}{4\ n_1^2} \qquad (3.9)$$

where NA is the numerical aperture $\sqrt{n_1^2-n_2^2}$ and n_1 and n_2 are refractive indexes of core and cladding respectively. Brinkmeyer (B1) also obtained a recaptured factor of the single-mode fiber, S_{single}, which is given by

$$S_{single} = \frac{3}{2n_1^2 w_0(\omega/c)} = \frac{3/2\ (NA)^2}{(w_0/a)^2 V^2\ n_1^2} \qquad (3.10)$$

where a is the core radius, V is the normalized frequency given by $kn_1 a\sqrt{2\Delta}$, w_0 is the spot size, ω and c are the angular frequency and speed of the light beam. For step-index S_{single} for variation of V values $1.5 \leq V \leq 2.4$ is given by

$$.21 \frac{(NA)^2}{n_1^2} \leq S_{single} \leq .24 \frac{(NA)^2}{n_1^2} \qquad (3.11)$$

Comparing (3.11) with (3.9) shows that S_{single} is not so different from S_{step} and S_{graded} if the NA is the same.

Rayleigh scattered light power from the entire fiber can be evaluated by integrating the fraction of the light power, reflected from an element that lies between ℓ and $\ell+d\ell$, over the entire length of fiber. Considering figure 3.3 and equation 3.7, the Rayleigh backscattered power can be shown as

$$p_{dist} = \int_0^L p(\ell)d\ell \qquad (3.12)$$

p_{dist} can also be symbolized as a phasor whose length corresponds to A_{dist} and whose angle with respect to the positive real axis corresponds to θ_{dist}, as shown in equation (3.13).

$$p_{dist} = A_{dist} \cos(\omega t - \theta_{dist}) \tag{3.13}$$

where

$$A_{dist} = \sqrt{X_1^2 + X_2^2} \tag{3.14}$$

$$\theta_{dist} = \text{Arctan}\frac{X_1}{X_2} \tag{3.15}$$

and

$$X_1 = \int_0^L p_0 \, S\alpha_s \exp(-2\alpha\ell) \sin\left(\frac{2n\omega\ell}{c}\right) d\ell \tag{3.16}$$

$$X_2 = \int_0^L p_0 \, S\alpha_s \exp(-2\alpha\ell) \cos\left(\frac{2n\omega\ell}{c}\right) d\ell \tag{3.17}$$

If we assume that α_s, α, and S are independent of position, A_{dist} and θ_{dist} can be written as

$$A_{dist} = \frac{p_0 S\alpha_s}{K_1^2+K_2^2} \sqrt{Y_1^2+Y_2^2}\,, \tag{3.18}$$

$$\theta_{dist} = \text{Arctan}\,\frac{Y_1}{Y_2} \tag{3.19}$$

where

$$Y_1 = \exp(K_1 L) \{K_1 \sin(K_2 L) - K_2 \cos(K_2 L)\} + K_2,$$

$$Y_2 = \exp(K_1 L) \{K_1 \cos(K_2 L) + K_2 \sin(K_2 L)\} - K_1,$$

$$K_1 = -2\alpha, \text{ and } K_2 = (2n\omega/c)$$

3.3 Combination of Fresnel and Rayleigh Reflections

In this situation Rayleigh reflections are not negligible compared with Fresnel echos or vice versa. The total reflected light power can be viewed as summation of two parts: (1) reflected power because of Rayleigh scattering designated by P_R. (2) Reflected power because of Fresnel reflections designated by P_F. Therefore, the total reflected power can be indicated by P_T and it can be formulated as

$$P_T = P_R + P_F \qquad (3.20)$$

3.3.1 Fresnel Reflections Power (P_F)

In (3.20) P_F itself can be expanded as

$$P_F = P_{F1} + P_{F2} + \ldots + P_{Fn} \qquad (3.21)$$

where P_{Fi} specifies the light power reflected from ith reflector along the fiber. If the fiber's properties are assumed to be uniform P_{Fi} can be shown by

$$P_{Fi} = A_{Fi} \exp(-2\alpha \ell_i) \cos(\omega t - \theta_{Fi}) \qquad (3.22)$$

where

$$A_{Fi} = p_0(1-T_i) \prod_{k=1}^{i-1} T_k^2 ,$$

$$\theta_{Fi} = \frac{2n\omega\ell_i}{c},$$

ℓ_i is the distance of ith reflector from the transmitter side, and T_i is the transmission coefficient of ith reflector.

Similar to what was shown in section 3.1 P_F can be converted to the form of

$$P_F = A_F \cos(\omega t - \theta_F) \qquad (3.23)$$

where

$$A_F = \sqrt{\{\sum_{i=1}^{n} A_{Fi} \exp(-2\alpha\ell_i) \sin\theta_{Fi}\}^2 + \{\sum_{i=1}^{n} A_{Fi} \exp(-2\alpha\ell_i) \cos\theta_{Fi}\}^2} \qquad (3.24)$$

$$\theta_F = \text{Arctan} \frac{\sum_{i=1}^{n} A_{Fi} \exp(-2\alpha\ell_i) \sin\theta_{Fi}}{\sum_{i=1}^{n} A_{Fi} \exp(-2\alpha\ell_i) \cos\theta_{Fi}} \qquad (3.25)$$

3.3.2 Rayleigh Reflections Power (P_R)

If reflectivity of discrete reflectors is assumed to be small, so that the transmitted light power decays exponentially along the fiber, resulting in the Rayleigh reflections power P_R can be expressed the same as shown in section 3.2. Therefore, P_R will be shown as

$$P_R = A_R \cos(\omega t - \theta_R) \qquad (3.26)$$

where A_R and θ_R are the same as A_{dist} and θ_{dist} respectively, revealed in section 3.2.

Now, the total reflected power P_T can be expressed as

$$P_T = A_T \cos(\omega t - \theta_T) \qquad (3.27)$$

where

$$A_T = \sqrt{(A_F\cos\theta_F + A_R\cos\theta_R)^2 + (A_F\sin\theta_F + A_R\sin\theta_R)^2} \qquad (3.28)$$

$$\theta_T = \text{Arctan}\ \frac{A_F \sin\theta_F + A_R \sin\theta_R}{A_F \cos\theta_F + A_R \cos\theta_R} \qquad (3.29)$$

CHAPTER IV

CALCULATED RESULTS

This chapter illustrates the calculated results of the reflections. Characteristics of discrete, distributed, and combination of discrete and distributed reflections are shown. The chapter continues with SNR calculation for OFDR. Also in this chapter, a comparative study with time domain technique is presented, and advantages/disadvantages of the frequency domain are discussed.

4.1 Characteristics of Discrete Reflections

Figures 4.1 through 4.6 show the phase, amplitude, and phasor-locus diagram of the reflected light power from a single-mode step-index fiber. For each figure there are different discrete reflectors along the fiber located at variety of positions from the transmitter side. The reflectivity of each reflector is assumed to be 0.1. The Rayleigh reflections are supposed to be negligible compared with Fresnel reflections. Figure 4.7 demonstrates the phase, amplitude, and phasor-locus diagram of the discrete reflections when the reflectivity of reflectors are not equal with

each other. In this figure there are three reflectors located at 100 (with reflectivity of 0.1), 200 (with reflectivity of .05), and 300 m (with reflectivity of .08) from the transmitter side. Figure 4.8 displays the phase, amplitude, and phasor-locus diagrams of discrete reflections when reflectors are not distributed uniformly.

The correspondence between phase and frequency is dependent upon the number of reflectors and their relative distances. The number of reflectors is shown by the number of peaks per cycle plus one on the phase graphs. The relative distances of each reflector corresponds with the frequency interval for each cycle such as

$$D = \frac{c}{2n\Delta f}$$

where D is the relative distance between two consecutive reflectors, Δf is the frequency interval for each cycle, n is the mean group index, and c is speed of light.

The reflectivity of each reflector can be approximated by maximum amplitude (A_{disc}) divided by the number of reflectors. In figure 4.1 one reflector is indicated by no peak per cycle. The distance of the reflector can be obtained by $(3 \times 10^8)/(2 \times 10^6 \times 1.48) \cong 100$ m. In figures 4.2 and 4.3, two and three reflectors with relative distances of 100 m are shown respectively.

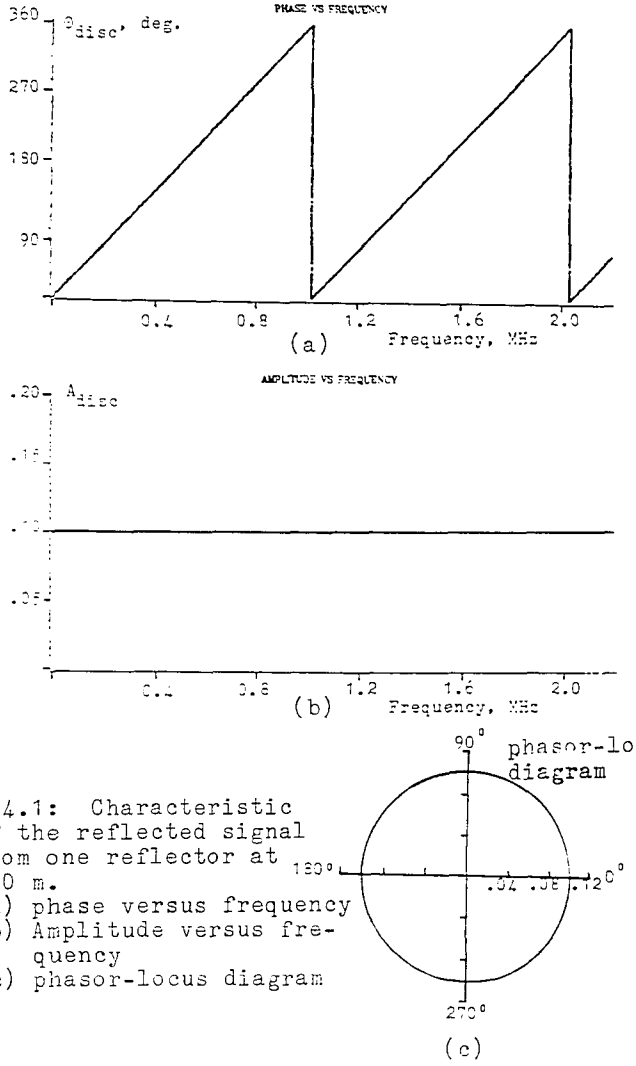

Figure 4.1: Characteristic of the reflected signal from one reflector at 100 m.
(a) phase versus frequency
(b) Amplitude versus frequency
(c) phasor-locus diagram

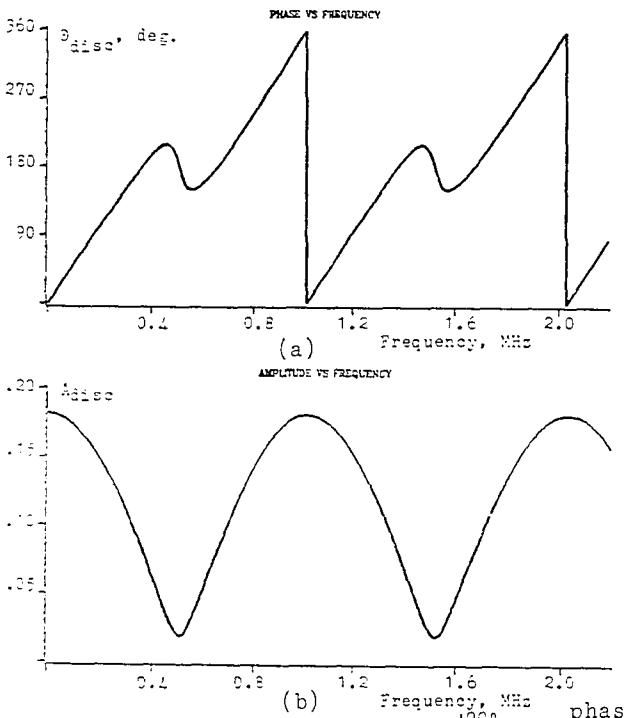

Figure 4.2: Characteristic of the reflected signal from two reflectors at 100 m and 200 m respectively from the fiber input end.
(a) phase versus frequency
(b) amplitude versus frequency
(c) phasor-locus diagram

phasor-locus diagram

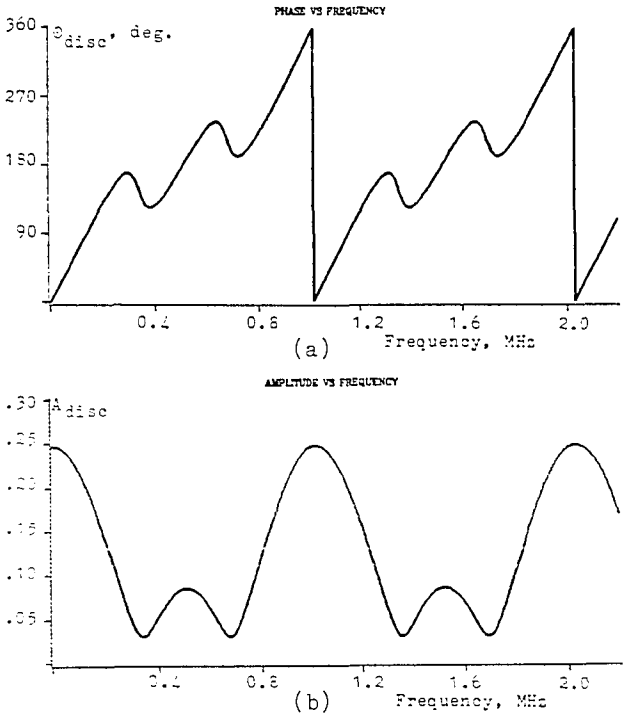

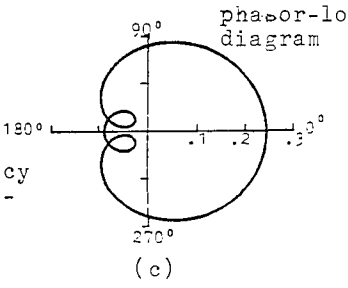

Figure 4.3: Characteristic of the reflected signal from three reflectors at 100m, 200m, and 300m respectively from the fiber input end.
(a) phase versus frequency
(b) amplitude versus frequency
(c) phasor-locus diagram

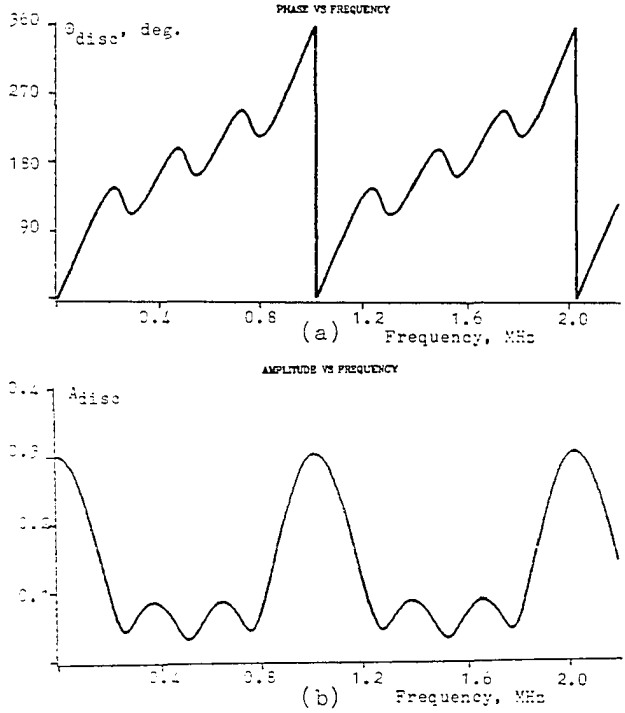

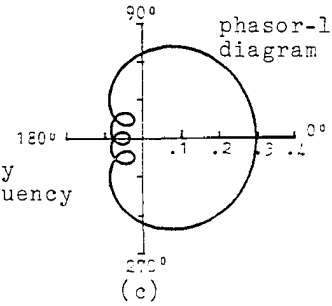

Figure 4.4: Characteristic phasor-locus diagram of the reflected signal from four reflectors at 100m, 200m, 300m, and 400m respectively from the fiber input end.
(a) phase versus frequency
(b) amplitude versus frequency
(c) phasor-locus diagram

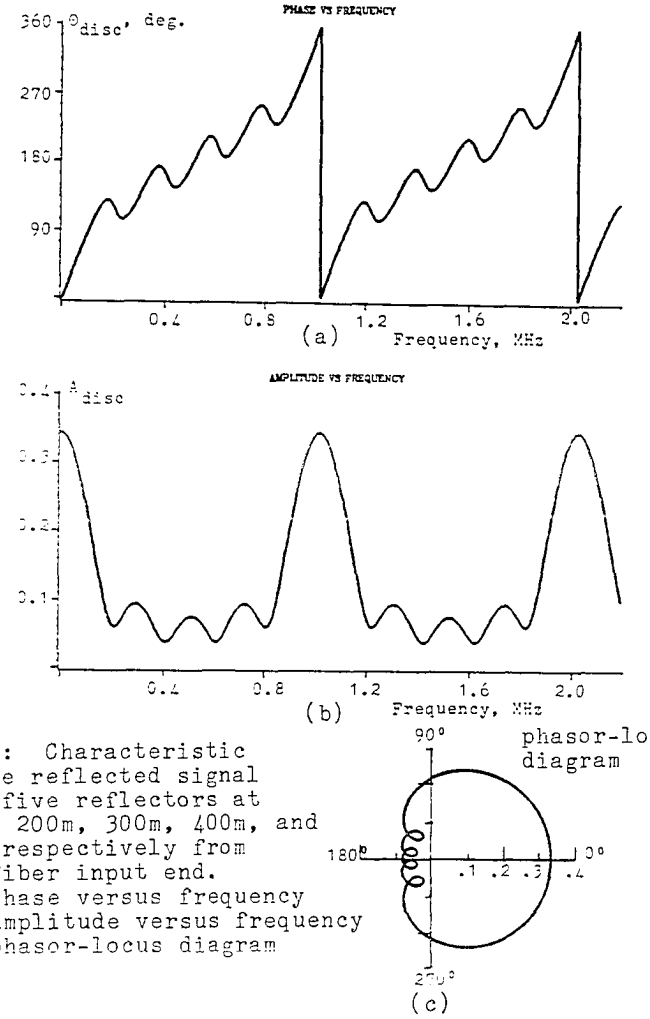

Figure 4.5: Characteristic of the reflected signal from five reflectors at 100m, 200m, 300m, 400m, and 500m respectively from the fiber input end.
(a) phase versus frequency
(b) amplitude versus frequency
(c) phasor-locus diagram

phasor-locus diagram

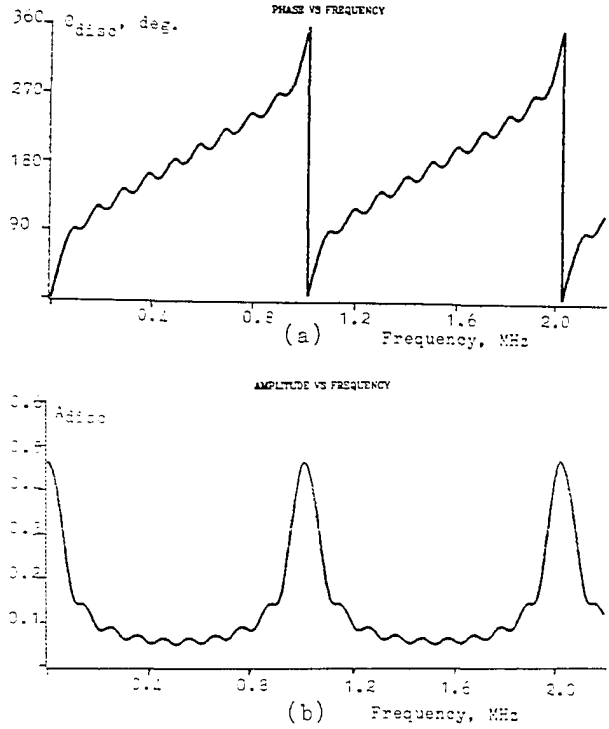

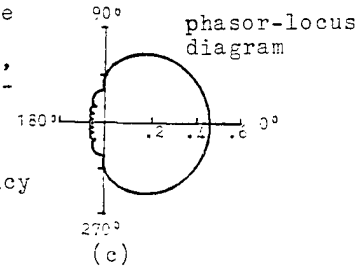

Figure 4.6: Characteristic of the reflected signal from ten reflectors at 100m, 200m, 300m,. . ., and 1000m respectively from the fiber input end.
(a) phase versus frequency
(b) amplitude versus frequency
(c) phasor-locus diagram

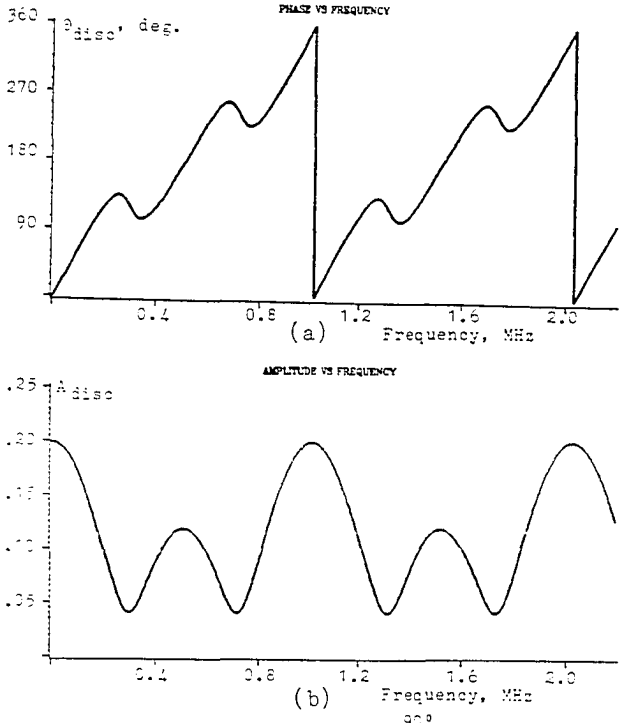

Figure 4.7: Characteristic of the reflected signal from three reflectors at 100m, 200m, and 300m with reflectiveties of 0.1, 0.05, and 0.08 respectively.
(a) phase versus frequency
(b) amplitude versus frequency
(c) phasor-locus diagram

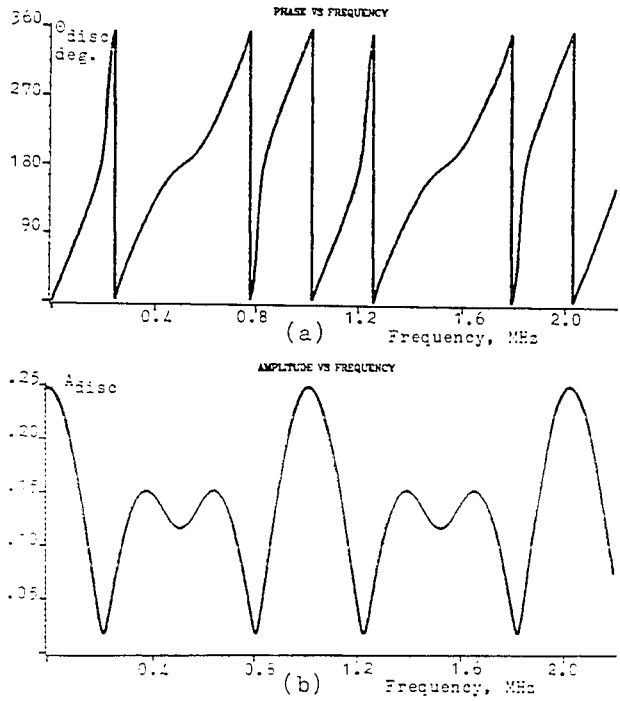

Figure 4.8: Characteristic of the reflected signal from three reflectors located at 100m, 300m and 400m with reflectiveties of 0.1
(a) phase versus frequency
(b) amplitude versus frequency
(c) phasor-locus diagram

4.2 Characteristics of Distributed Reflections

Figure 4.9 illustrates the phase, amplitude, and phasor form of the distributed reflections from a 500 m multimode fiber. The ratio of the relative signal strength of Rayleigh reflections is assumed to be much higher than Fresnel reflections. Fiber's properties are supposed to be uniform and parameters are as follows:

$\alpha = 2 \times 10^{-3}$ nepers/meter ($\sim$ 9 dB/km)

$\alpha = \alpha_s$ (Rayleigh scattering only), and $S = 5 \times 10^{-3}$ (recaptured factor)

Due to small amplitude for higher frequencies, OFDR is an inadequate technique for determining distributed reflections.

4.3 Characteristics of Combination of Discrete and Distributed Reflections

Figure 4.10 shows the phase, amplitude, and phasor-locus diagram of the combination of Fresnel and Rayleigh reflections from a 500 m multimode fiber. Fiber's properties are assumed to be uniform and parameters are as follows:

$\alpha_s = 2 \times 10^{-3}$ nepers/meter ($\sim$ 9 dB/km),

$\alpha = \alpha_s$

$S = 5 \times 10^{-3}$, and end reflectivity = 0.01.

We can see the distributed reflections are noticeable up to 0.6 MHz. Above 0.6 MHz the end reflections are most noticeable.

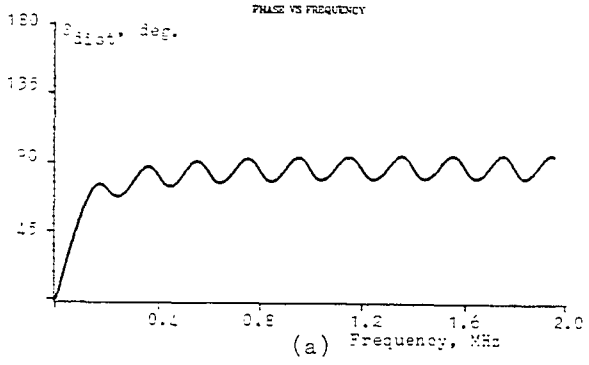

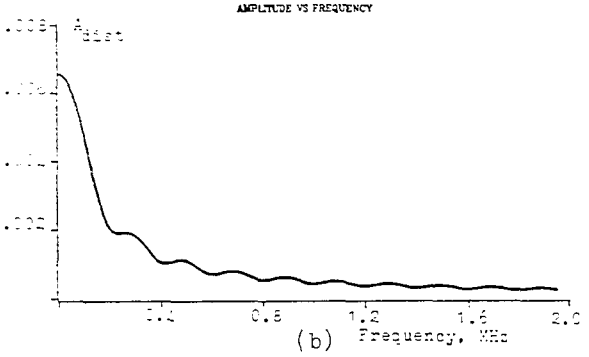

Figure 4.9: Characteristic of the distributed reflections from a 500 m fiber.
(a) phase versus frequency
(b) amplitude versus frequency
(c) phasor-locus diagram

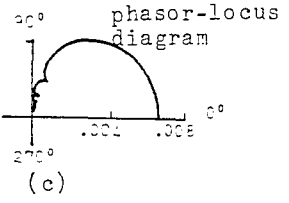

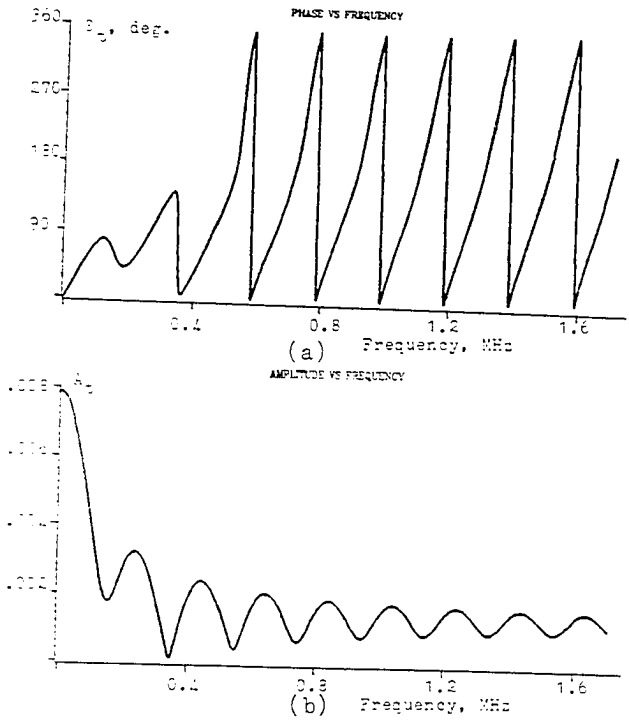

Figure 4.10: Characteristic of the combination of distributed and discrete reflections from a 500 m fiber.
(a) phase versus frequency
(b) amplitude versus frequency
(c) phasor-locus diagram

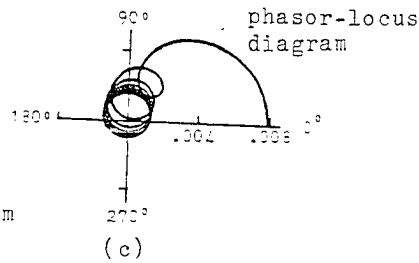

4.4 Randomly Distributed Reflections

Disbributed reflections normally can be characterized as echos from randomly distributed reflectors along the fiber. In this case, for high values of scattering loss, phase and amplitude of echos will behave randomly at high frequencies. The amplitude of reflections will not approach zero uniformly. Figures 4.11 through 4.13 show the characteristic of randomly distributed reflections from three 500 m fibers. It is assumed light backscatters randomly along the fiber and the average scattering loss is different for each fiber. In fibers with low loss, amplitude and phase are changing periodically, and the frequency interval of each cycle depends upon the fiber length. For fibers with higher scattering loss, the periodic behavior of phase and amplitude approaches a random process.

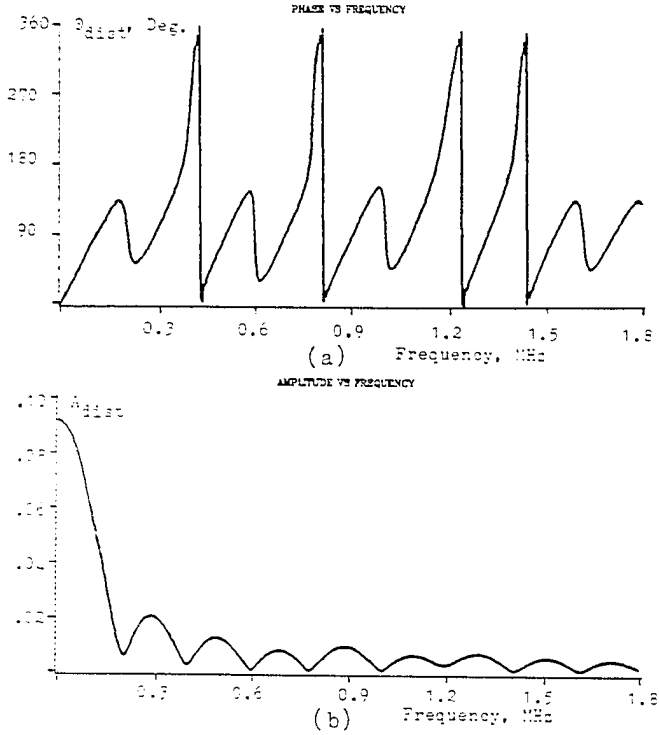

Figure 4.11: Characteristic of the randomly distributed reflections from a 500 m fiber with average loss of 0.8 dB/km.
(a) phase versus frequency
(b) amplitude versus frequency
(c) phsor-locus diagram

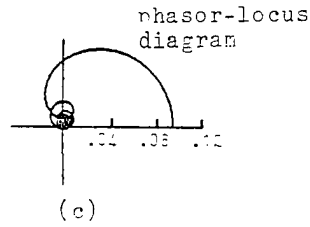

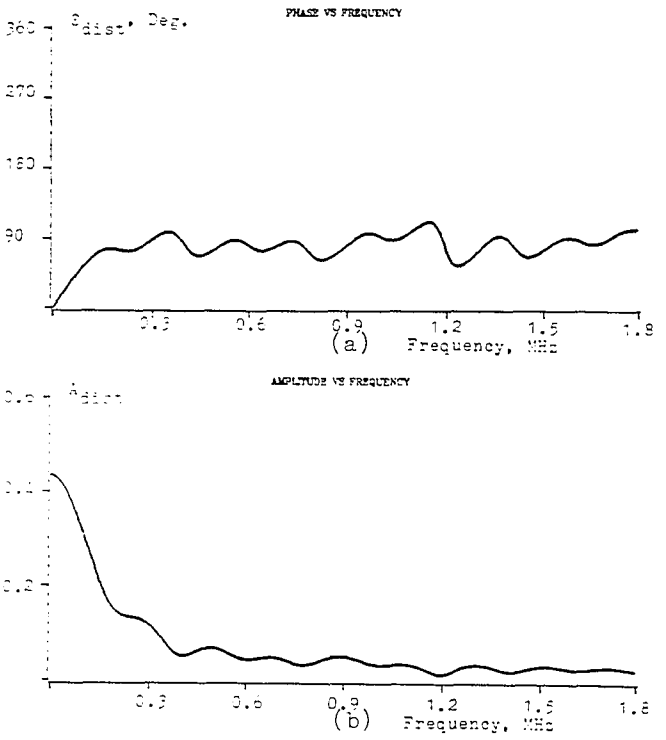

Figure 4.12: Characteristic of the randomly distributed reflections from a 500 m fiber with average loss of 4 dB/km.
(a) phase versus frequency
(b) amplitude versus frequency
(c) phasor-locus diagram

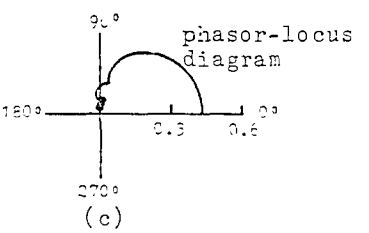

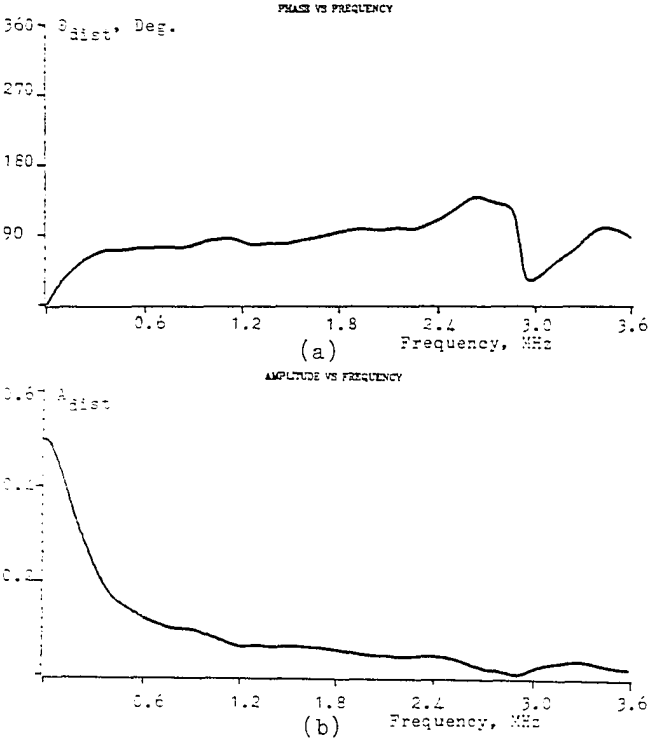

Figure 4.13: Charactristic of the randomly distributed reflections from a 500 m fiber with average loss of 7 dB/km.
(a) phase versus frequency
(b) amplitude versus frequency
(c) phasor-locus diagram

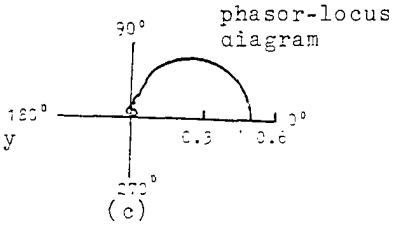

4.5 Signal to Noise Ratio (SNR) of the OFDR

In order to estimate the SNR of the OFDR shown in figure 4.14, it is assumed that the incident and reflected waves are sinusoidally intensity modulated. The photocurrent generated by the reflected light is given by (Y1)

$$i_s(t) = \frac{e\eta}{h\nu} P_r (1 + m \cos(\omega t - \theta)) \qquad (4.1)$$

where e is electron charge, η is quantum efficiency of photodiode, h is Planck's constant (6.625×10^{-34} J-s), ν is the frequncy of light beam, P_r is the mean value of the reflected optical power, and m is modulation index. The received signal power is proportional to the mean-squre value of the photocurrent. Therefore, the mean-square value of sinusoidal cuurrent component will be

$$\bar{i}_s^2 = \left(\frac{e\eta m P_r}{h\nu\sqrt{2}}\right)^2 \qquad (4.2)$$

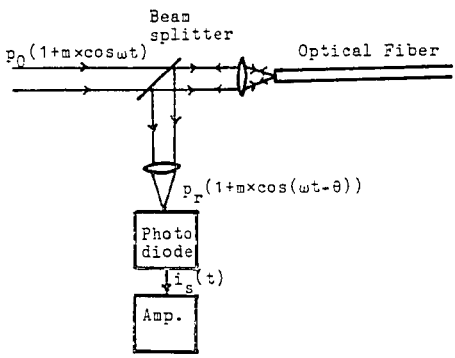

Figure 4.14: Schematic diagram of an OFDR.

It is postulated that there are two noise sources. The first one is shot noise associated with random generation of carriers. It has mean-square value of (Y1)

$$\bar{i}_{ns}^2 = 2e\bar{I}\Delta f \qquad (4.3)$$

where $\bar{I}$ is the average current of photodiode. From equation 4.1, it is given by

$$\bar{I} = \frac{e\eta P_r}{h\nu} \qquad (4.4)$$

Δf is the bandwidth of the receiver. The second noise source is the thermal noise generated by output load of the photodiode. It has a mean-square value of (Y1)

$$\bar{i}_{nt}^2 = \frac{4kT_e\Delta f}{R_L} \qquad (4.5)$$

where T_e is equivalent input noise temperature of the receiver following the photodiode. R_L is the receiver's input resistance. k is Boltzmann's constant (1.38×10^{-23} J/K). The signal to noise ratio introduced to the receiver is thus

$$\frac{S}{N} = \frac{\bar{i}_s^2}{\bar{i}_{ns}^2 + \bar{i}_{nt}^2} \quad \frac{\frac{1}{2}(e\eta/h\nu\ mP_r)^2}{(2e^2\eta P_r/h\nu)\Delta f + (4kT_e/R_L)\Delta f} \qquad (4.6)$$

The result of SNR calculation as a function of fiber length is shown in figure 4.15. The values of parameters used for

the calculation are as follows

Fiber loss, α	0.8	dB/km
Rayleigh scattering loss, α_s	0.5	dB/km
Fiber's end reflectivity, R	0.05	
Quantum efficiency, η	60%	
Load resistance, R_L	50	Ω
Receiver bandwidth, Δf	1	kHz

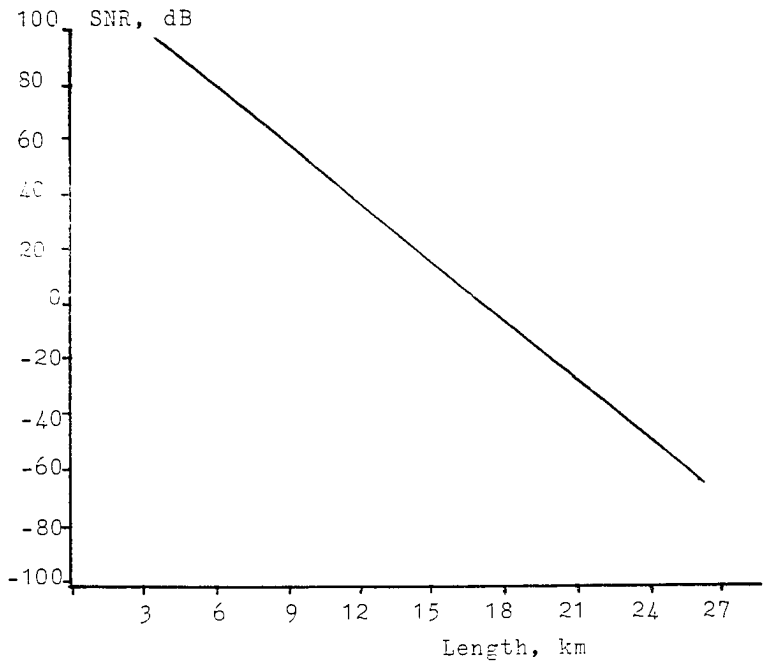

Figure 4.15: SNR of the reflected signal as a function of fiber length

The power required to generate nonlinear frequency component such as Stimulated Raman Scattering (SRS) (M4) is known as the critical power. This threshold power is calculated by Smith (S4)

$$P_{crit} = \frac{16\ A_{eff}}{L_{eff}\ g_0} \qquad (4.7)$$

A_{eff} is an effective core area given by (M4)

$$A_{eff} = 2\pi w_n^2 \qquad (4.8)$$

$$w_n = a(0.65+1.619/V^{3/2}+2.879/V^6)$$

a is the core radius and V is the normalized frequency. L_{eff} in (4.7) is an effective length given by (I1)

$$L_{eff} = \frac{1-e^{-\alpha L}}{\alpha} \qquad (4.9)$$

where αL is the total attenuation in nepers. For long length of fiber where material dispersion is sufficiently small, L_{eff} is approximately equal to $1/\alpha$. g_0 is called the Raman gain coefficient and it is given by (M4).

$$g_0 = 9.78 \times 10^{-14}/\lambda \quad m/W \qquad (4.10)$$

The critical power as a function of wavelength for a typical fiber used in this research is shown in figure (4.16).

4.6 Detection of Returned Signal in the Presence of Noise

Consider now the detection of reflected signal when it is contaminated by additive noise n(t). Since the receiver

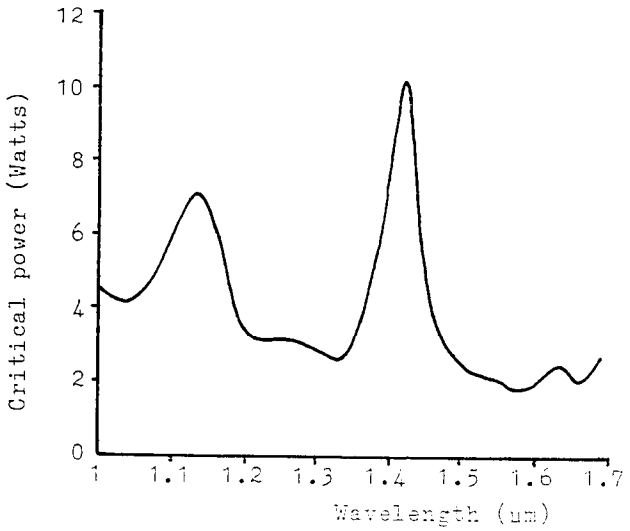

Figure 4.16: Critical power as a function of wavelength for a typical single-mode fiber

used in OFDR is a narrowband receiver, n(t) can be considered as a narrowband noise. According to equation (4.1) the sinusoidal photocurrent component plus a narrowband noise n(t) can be presented as

$$i(t) = \frac{e\eta}{h\nu} mP_r \cos(\omega t+\theta) + n(t) \qquad (4.11)$$

The zero-mean narrowband noise is expressible as

$$n(t) = x(t) \cos\omega t - y(t) \sin\omega t \qquad (4.12)$$

where x(t) and y(t) have also zero-mean. n(t) can also be expressed as

$$n(t) = z(t)\cos(\omega t+\theta_n) \qquad (4.13)$$

where $z(t)=(x^2+y^2)^{\frac{1}{2}}$ and $\theta_n=\text{Arctan}\ \frac{y}{x}$

Physically we expect noise affects the amplitude and phase of the returned signal. If the rms noise amplitude is much less than signal amplitude itself, the niose will have a small effective phase and amplitude deviation. conversely, if the noise is large, signal suppression must be expected.

Proceeding to the analysis, the receiver input is

$$i(t) = \frac{e\eta}{h\nu} mP_r \cos(\omega t+\theta) + z(t)\cos(\omega t+\theta_n) \qquad (4.14)$$

After a little manipulation, i(t) can be written in the form

$$i(t) = r(t)\cos\{\omega t+\psi(t)\} \qquad (4.15)$$

where

$$r(t)=\sqrt{(I_s\sin\theta+z\sin\theta_n)^2+(I_s\cos\theta+z\cos\theta_n)^2} \qquad (4.16)$$

$$\psi(t)=\text{Arctan}\ \frac{I_s\ \sin\theta\ +z\ \sin\theta_n}{I_s\ \cos\theta\ +z\ \sin\theta_n} \qquad (4.17)$$

$$I_s = \frac{e\eta}{h\nu} mP_r$$

The detected amplitude and phase are equal to r(t) and $\psi(t)$ shown in equations (4.16) and (4.17) respectively. But in view of the complexity of r(t) and $\psi(t)$, as written above, useful expressions for the output call for some simplifying approximations. Therefore, it can be assumed the signal is either very large or very small compared to the noise, such that $I_s >> z$ or $I_s << z$ most of the time. These are equivalent to $(S/N) >> 1$ or $(S/N) << 1$. The phasor constructions of figure 4.17, where the phase angle ωt common to both i(t) and n(t) has been taken as the reference, lead to the approximations

$$\psi = \theta + \frac{z}{I_s} \sin\phi \quad \text{and} \quad r(t) = \{I_s^2 + z^2 \sin^2\phi\}^{\frac{1}{2}} \quad \text{for } (S/N) >> 1 \qquad (4.18)$$

$$\psi = \theta_n - \frac{I_s}{z} \sin\phi \quad \text{and} \quad r(t) = \{I_s^2 \sin^2\phi + z^2\}^{\frac{1}{2}} \quad \text{for } (S/N) << 1 \qquad (4.19)$$

where $\phi = \theta_n - \theta$

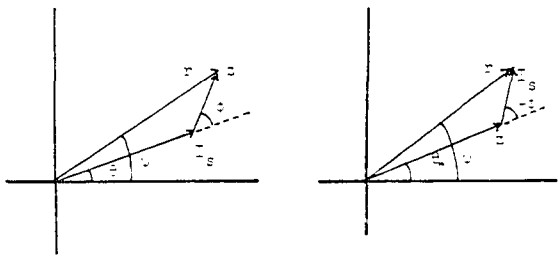

Figure 4.17: Phasor diagram for reflected signal in the presence of noise

A careful examination of equations (4.18) and (4.19) reveals that for (S/N)>>1 the detected phase and amplitude are almost equal to the phase and amplitude of the returned signal. But for (S/N)<<1 the returned signal phase θ appears only as part of $\sin\phi$, which also includes θ_n and in turn is multiplied by the random variable 1/z. This means that the returned signal's properties are multilated by noise and cannot be recovered. The resulting threshold effect is a serious problem in detecting of phase and amplitude. Figures 4.18 and 4.19 show the returned signal characteristics from discrete reflections in the presence of the noise. Figure 4.20 reveals the characteristics of the distributed reflections from a 500 m fiber with α=0.002 nepers/m when the maximum SNR at the receiver input is about 10 dB. At frequencies above 0.4 MHz, SNR becomes very small (about -5 dB). Therefore, no information can be obtained from the reflected signal. Figure 4.21 explains the phase, amplitude, and phasor-locus diagram of the combination of distributed and end reflections from a 500 m fiber. Presence of end reflection in the returned signal causes the SNR to be high enough at frequencies above 0.4 MHz. The detected phase behaves approximately the same as theory expressed in equation (3.29).

4.7 Comparison Between Time Domain and Frequency Domain Techniques

Time and frequency domain techniques can both be used for the study of fault location. But in some other cases

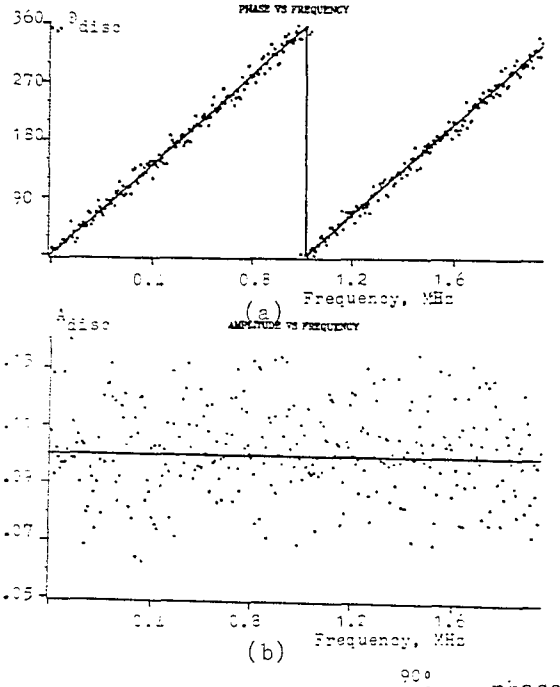

Figure 4.18: Characteristic of the reflected signal from one reflector located at 100 m when S/N=12 dB
(a) phase versus frequency
(b) amplitude versus frequency
(c) phasor-locus diagram

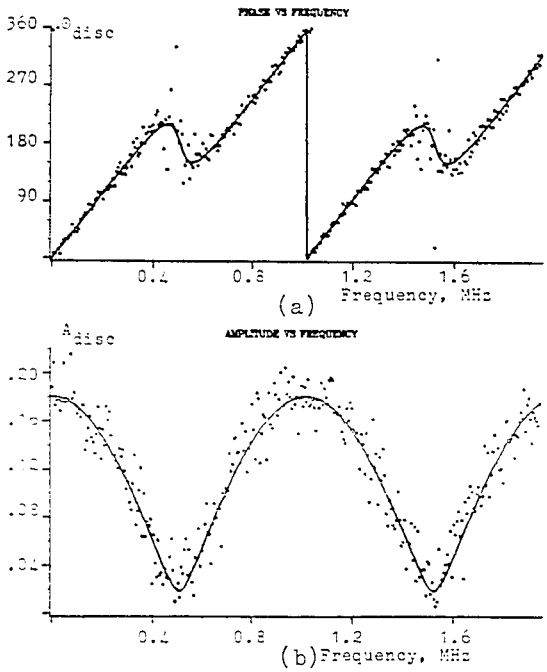

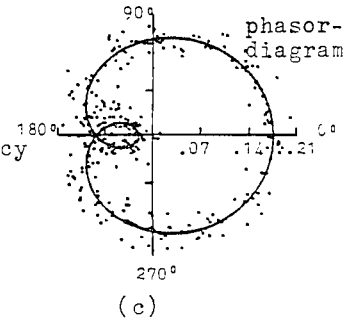

Figure 4.19: Characteristic phasor-locus diagram of the reflected signal from two reflectors at 100 m and 200 m when S/N=20 dB.
(a) phase versus frequency
(b) amplitude versus frequency
(c) phasor-locus diagram

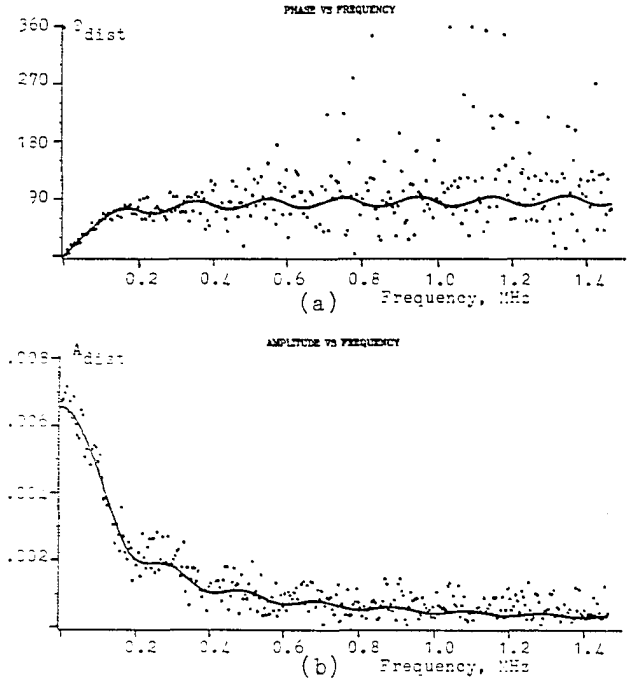

Figure 4.20: Characteristic of the distributed reflections from a 500 m fiber with α_s=0.002 nepers/m and average S/N=10 dB
(a) phase versus frequency
(b) amplitude versus frequency
(c) phasor-locus diagram

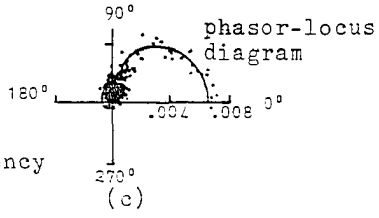

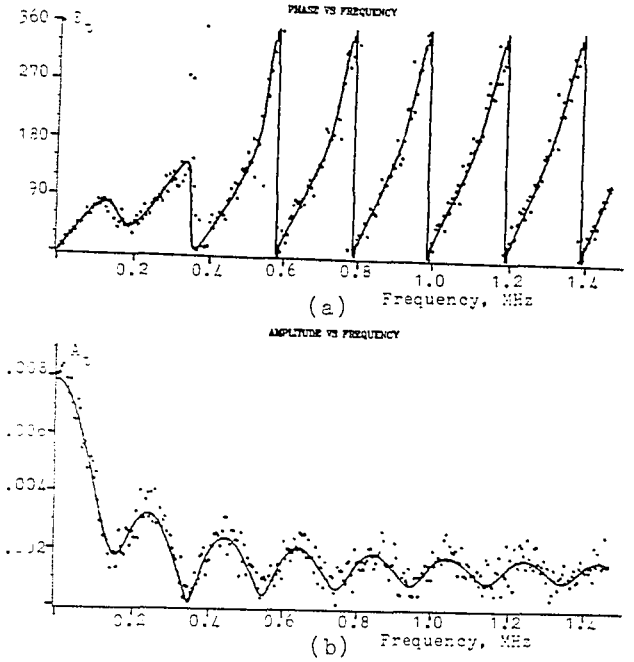

Figure 4.21: Characteristic of the combination of distributed and discrete reflections from a 500 m fiber with α_s=0.002 nepers/m and average $\bar{S}/N$=10 dB
(a) phase versus frequency
(b) amplitude versus frequency
(c) phasor locus diagram

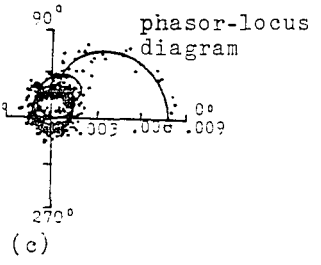

such as SNR improvements, distance resolution, discrete reflections, characterizing fiber parameters, etc. one technique has advantages over the other. Which technique is preferable depends on the kind of experiment and instrumentation that is most easily available. Time domain technique require the availability of means for producing and detecting short pulses (nanosecond durations). Frequency domain measurement, on the other hand, require a signal generator that is tunable from dc to the several hundred MHz frequency range for driving a light modulator that also must be able to cover the same frequency range. Each technique requires sophisticated equipment, so that the final choice is dependent upon the experiment, experimenter's preference, or the availability of equipment.

4.7.1 SNR Improvement

In order to compare the SNR of frequency domain (SNR_f) and time domain reflectometry techniques (SNR_t) we consider the following factors to be equal in both systems: the rms launched signal power, the beam splitter ratio, and the optical equivalent receiver noise power. Assuming that the receivers of both systems differ only in bandwidth, the ratio M of SNR of a frequency domain system to that of a time domain system can be shown as

$$M = \left(\frac{R_f}{R_t}\right)^2 \frac{B_t}{B_f} \qquad (4.20)$$

where B_f and B_t are the bandwidth of the receivers of the frequency domain and time domain reflectometers respectively. R_f and R_t are reflection coefficients for the two systems but they are not the same because of the frequency dependence of reflections in frequency domain technique shown in chapter 3. Figures 4.22 through 4.24 show ratio M in dB as a function of frequency for three different fibers. These figures show that the average SNR_f is higher than average SNR_t.

For the OFDR used in this research it is possible to make the detector bandwidth arbitrarily small, because the spectrum of the sinusoidal signal consists only one discrete line, and the spectrum of reflected signal is thus also one discrete line. As a result, the SNR can be improved by reducing the receiver bandwidth. In time domain technique, however, the SNR can be improve by averaging. There are two averaging methods. One is the digital averaging method, and the other is an analog averaging method using a boxcar integrator. In the digital method, the averaging operation samples the signal repeatedly in a narrow time slot and rescues the signal from the large background noise by summing over all the samples. Randomly phased noise cancels during the summation process while the signal adds coherently and builds up. The time slot used for taking the samples is slowly moved across the entire temporal range that is to be examined. Okada has reported that SNR improvement value is 50 dB when a 8 bit high speed digital averager is used (01).

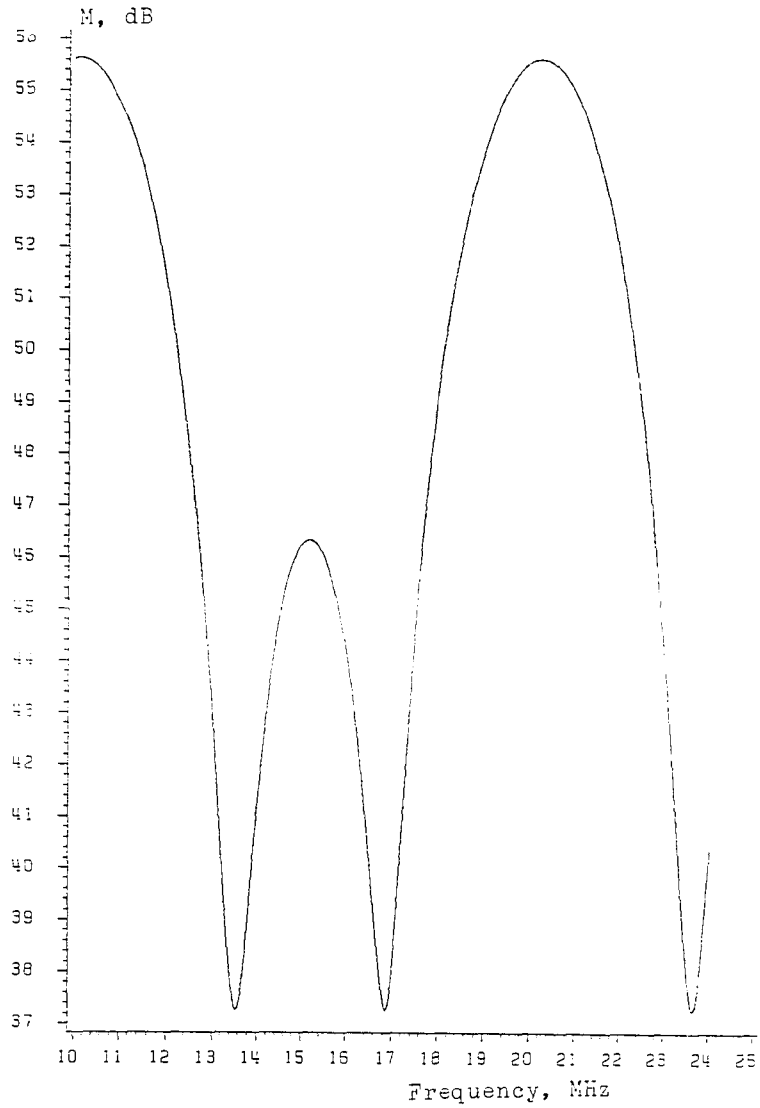

Figure 4.22: Graph of M as a function of frequency for three discrete reflectors

B_f=100 Hz B_t=1 MHz

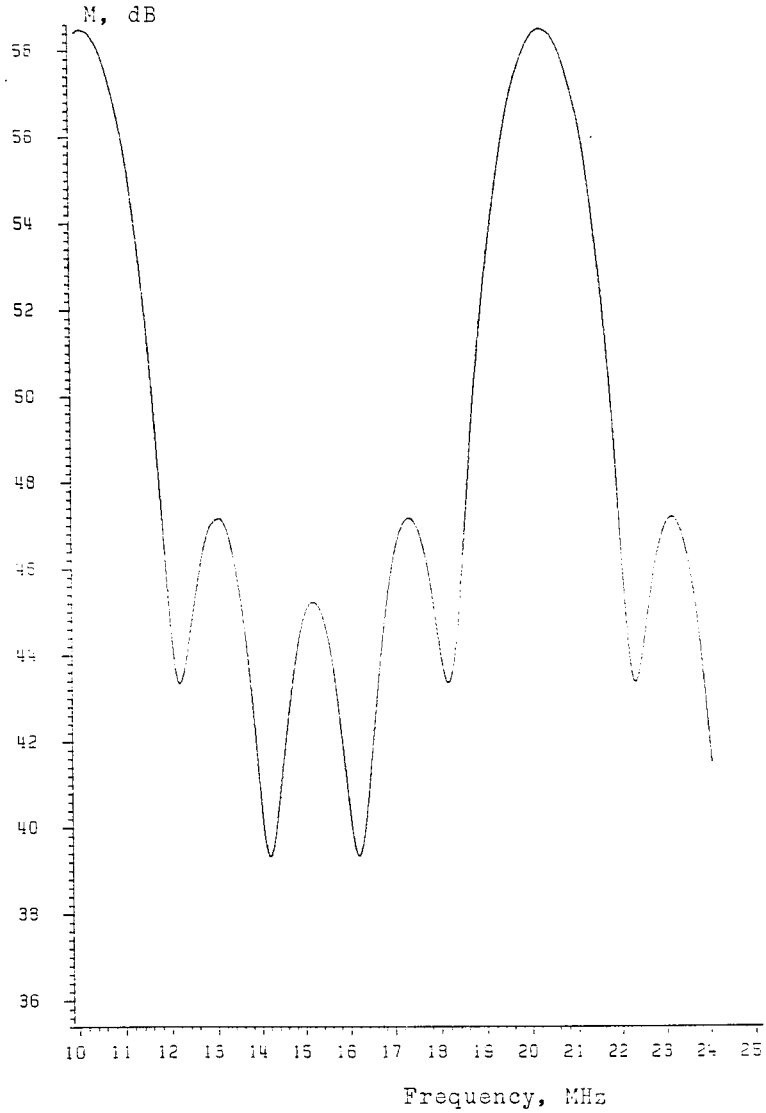

Figure 4.23: Graph of M as a function of frequency for five discrete reflectors

B_f=100 Hz B_t=1 MHz

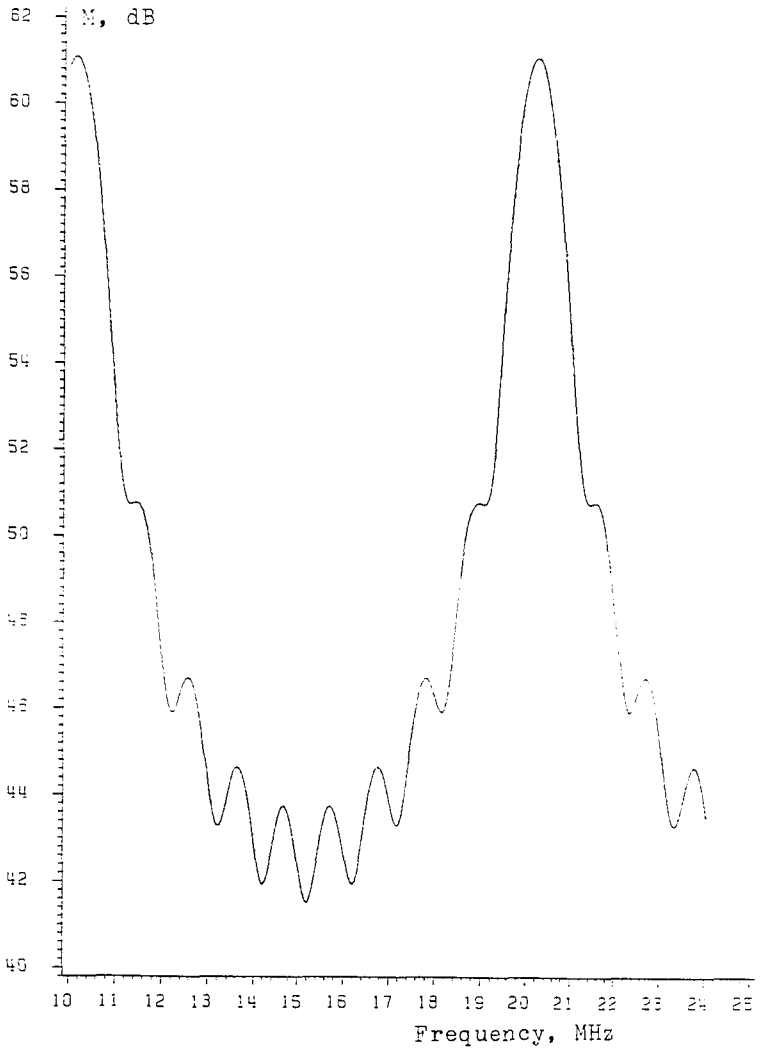

Figure 4.24: Graph of M as a function of frequency for ten discrete reflectors

B_f=100 Hz B_t=1 MHz

4.7.2 Discrete Reflections

One of the advantages of frequency domain technique over the time domain technique is where the detection of discrete reflections is specifically required. The back-scattered signal for OFDR is frequency dependent (shown in equation 3.13). For low modulation frequencies the back-scattered signals will add up and the signal strength will build up. For high frequencies, however, they will de-structively interfere. As a result, in the case of the combination of discrete and distributed reflections, the distributed reflections will not appreciably affect the returned signal for high modulation frequencies. This situation can help an experimenter to delete the backscattering effect when discrete reflections are specifically required for detection. Figure 4.10 is a good example of a 500 m fiber with both Rayleigh and Fresnel reflections. For low frequencies, Rayleigh reflections contribute significantly to the returned signal. But, for frequencies above 0.4 MHz, only reflections from the fiber end are detected.

4.7.3 Testing the Fiber Parameters Along the Z-Axis

In general OFDR is not suitable for any experiment which requires detection of distributed reflections. An example of these experiments is characterizing fiber parameters along the z-axis (z is the coordinate along the direction of propagation). Similar to what was mentioned in section 4.7.2, distributed reflections build up only at low frequencies.

They have a very low amplitude for high frequencies. The OTDR is probably the most useful tool for studying the fiber parameters which involve backscattering.

CHAPTER V

DISCUSSION

5.1 Frequency Effect on the Returned Signals

On the basis of the results of the previous chapters, the OFDR appears to have advantages over the OTDR when the discrete reflections are specifically required for detection. Unlike the time domain technique, in frequency domain the returned signals are in the steady state condition. Therefore, discrete and distributed reflections cannot be extracted from the returned signal. It is known, however, that Rayleigh reflections will build up only in low frequencies. In the other words, they have high/low amplitude for low/high frequencies. Figures 5.1 and 5.2 represent the Rayleigh reflections as a function of frequency for different fibers with various attenuation factors and lengths. The fiber ends are assumed to immersed into a matching oil that causes no Fresnel reflection from the ends. The reflected signal amplitude approaches zero as frequency increases. For the fibers with higher/lower α (α is attenuation loss), returned signal amplitude will reach zero at higher/lower

frequencies. Figures 5.3 and 5.4 represent the reflections from the same fibers used in figures 5.1 and 5.2 except all fibers are assumed to have an end reflectivity of 0.1. Therefore, at low frequencies distributed reflections dominate the reflected signal, whereas at high freguencies Fresnel reflections are the major contributor. These figures also indicate that reflections from fiber ends (which are observed in high frequencies) will have higher amplitude for fibers with lower α.

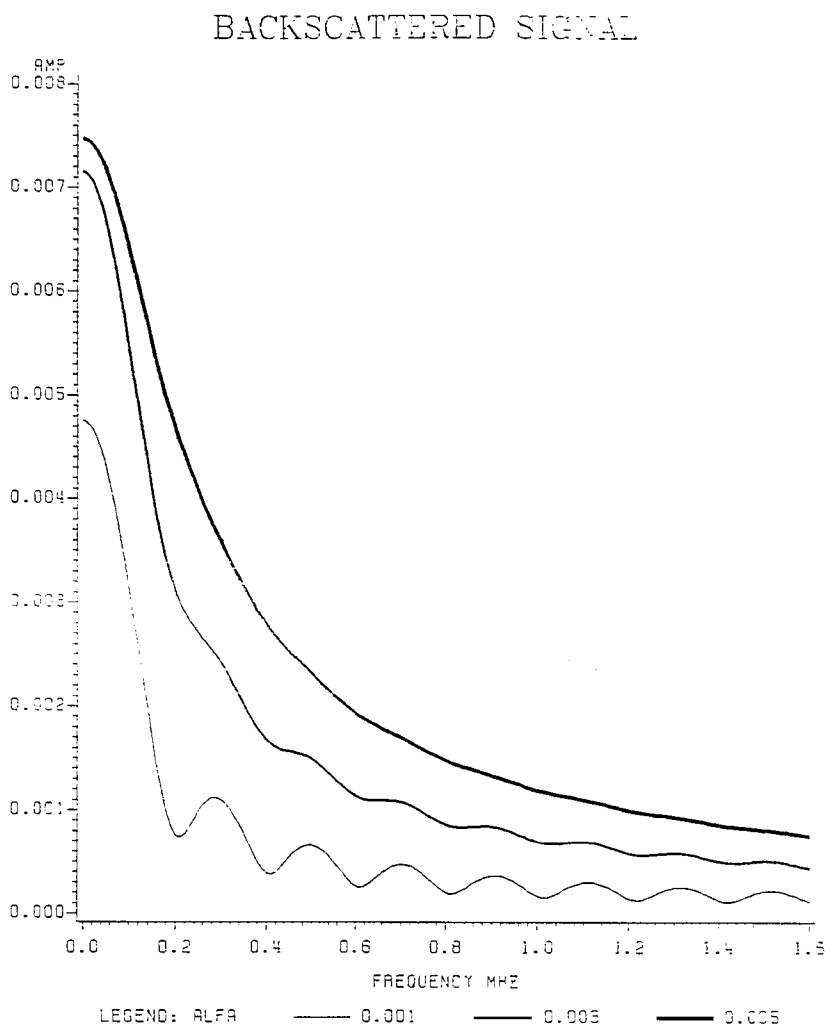

Figure 5.1: Backscattered signal amplitude versus frequency for a 500 m fiber with no end reflections

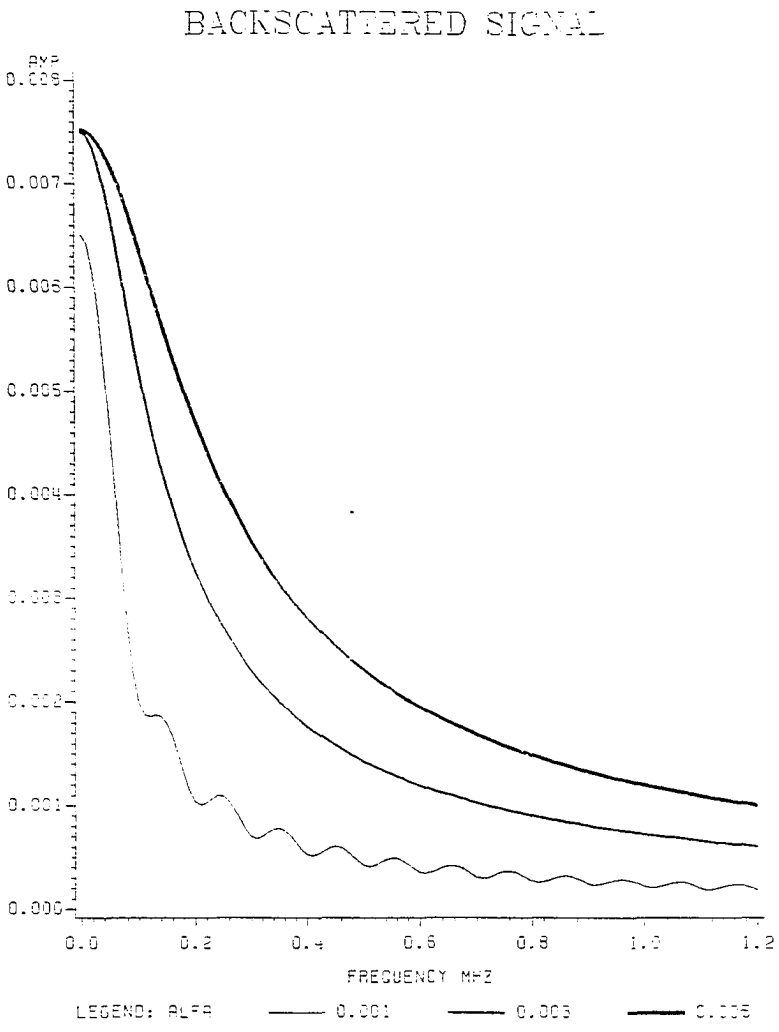

Figure 5.2: Backscattered signal amplitude versus frequency for a 1000 m fiber with no end reflections

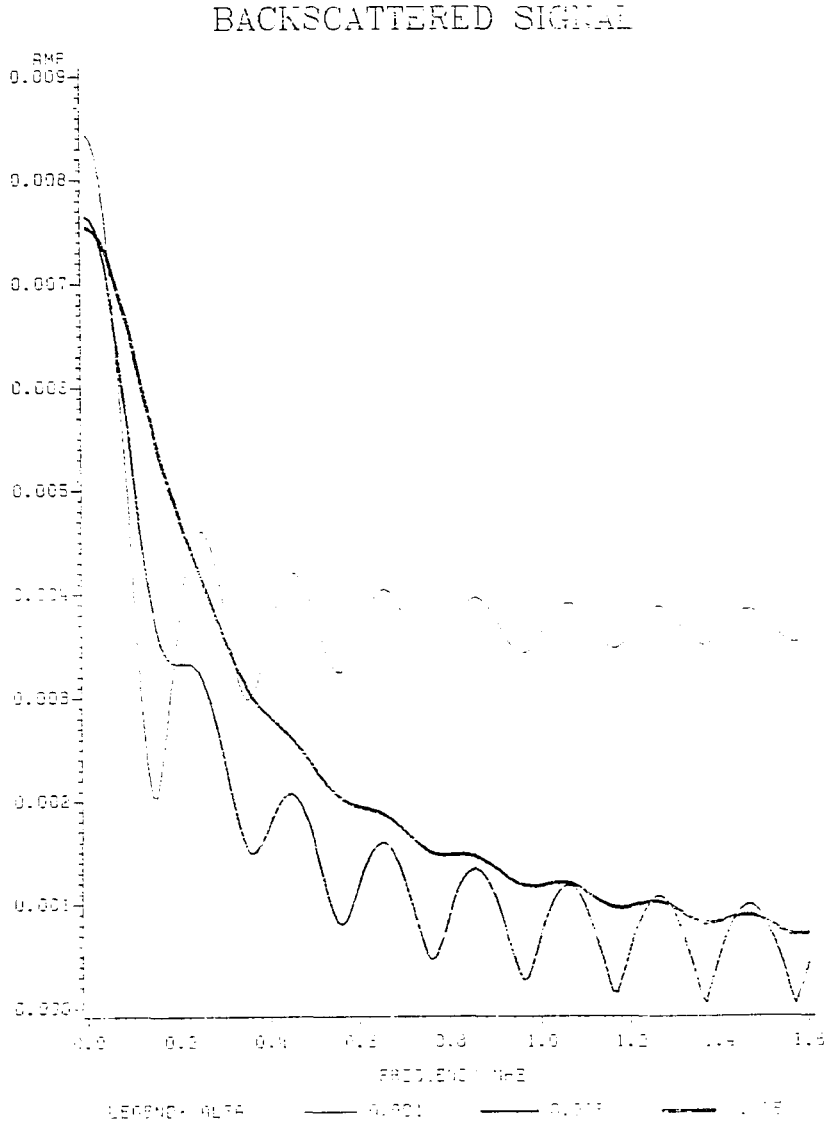

Figure 5.3: Backscattered signal amplitude versus frequency for a 500 m fiber with end reflectivity of 0.01

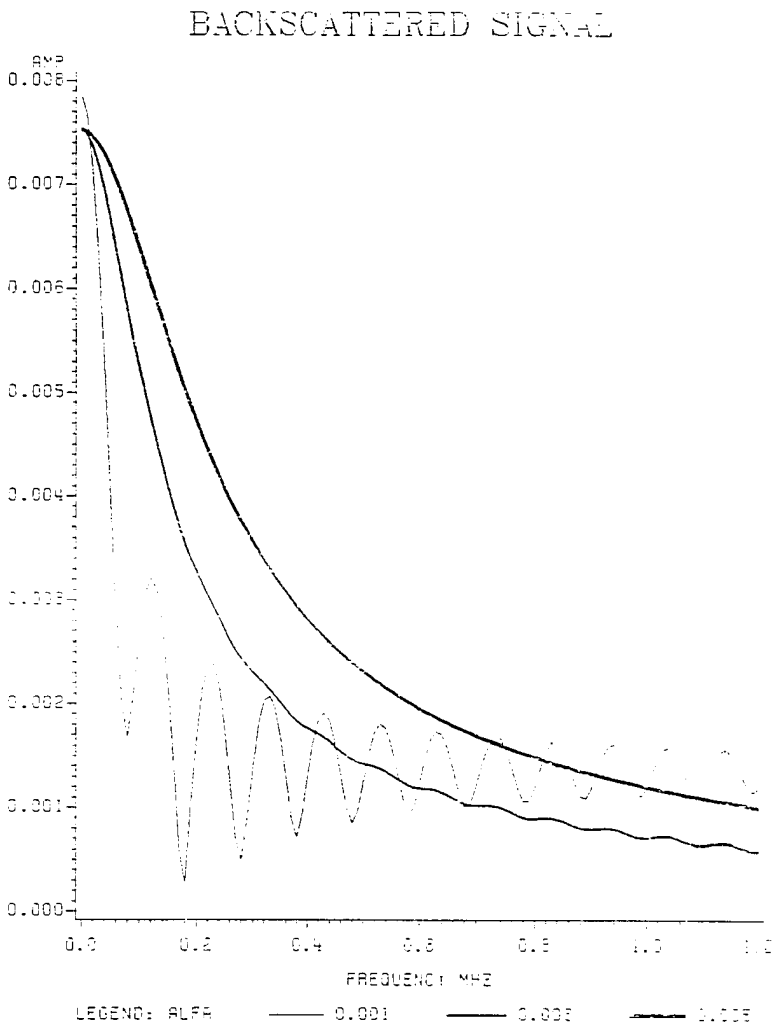

Figure 5.4: Backscattered signal amplitude versus frequency for a 1000 m fiber with end reflectivity of 0.01

5.2 Distributed to Discrete Reflections Ratio

It is very important to recognize the percentage of each type of reflection in the returned signal. There are some parameters which control the amount of the distributed and discrete reflections at the receiver side. The most important ones are:

(1) Fiber scattering loss α_s

(2) Fiber attenuation loss α

(3) Length of the fiber

(4) Frequency of modulation

(5) S factor (portion of the scattered light guided back towards the transmitter)

(6) Reflectivity of each discrete reflector

To analyse the sensitivity of each type of reflection to the above mentioned parameters, the ratio of Rayleigh reflections to the Fresnel reflections are defined as follow:

$$\text{RATIO} = \frac{P_R}{P_F} \qquad (5.1)$$

where P_R and P_F are defined by equations (3.23) and (3.26).

5.2.1 Effect of Length and α on RATIO

RATIO strongly depends on α and length of the fiber. Figures 5.5 through 5.7 represent this dependency at three different frequencies. The graphs are prepared for fibers whose lengths range from 500 to 1500 meters and α is in the range of 5×10^{-4} to 2×10^{-3} nepers/m (2.1 to 8.6 dB/km attenua-

tion) The end reflectivity and S factor of each fiber is assumed to be 0.1 and 0.02 respectively.

Figure 5.5 is for a modulation frequency of 50 kHz. As it shows, for α higher than 10^{-3} nepers/m and lengths higher than 800 m, the RATIO is higher than 10. This means for α and lengths below those values, RATIO will drop to the smaller values with a minimum of 0.6 at $\alpha=5\times10^{-4}$ and length=500 m.

Figures 5.6 and 5.7 represent the RATIO for fibers with the same parameters of figure 5.5 except the modulation frequency for figure 5.6 is 0.1 and for figure 5.7 is 0.5 MHz. As mentioned before, at higher frequencies Rayleigh reflections will not dominate the returned signal strength as they do for lower frequencies. Therefore, the RATIO will approach zero as the frequency increases.

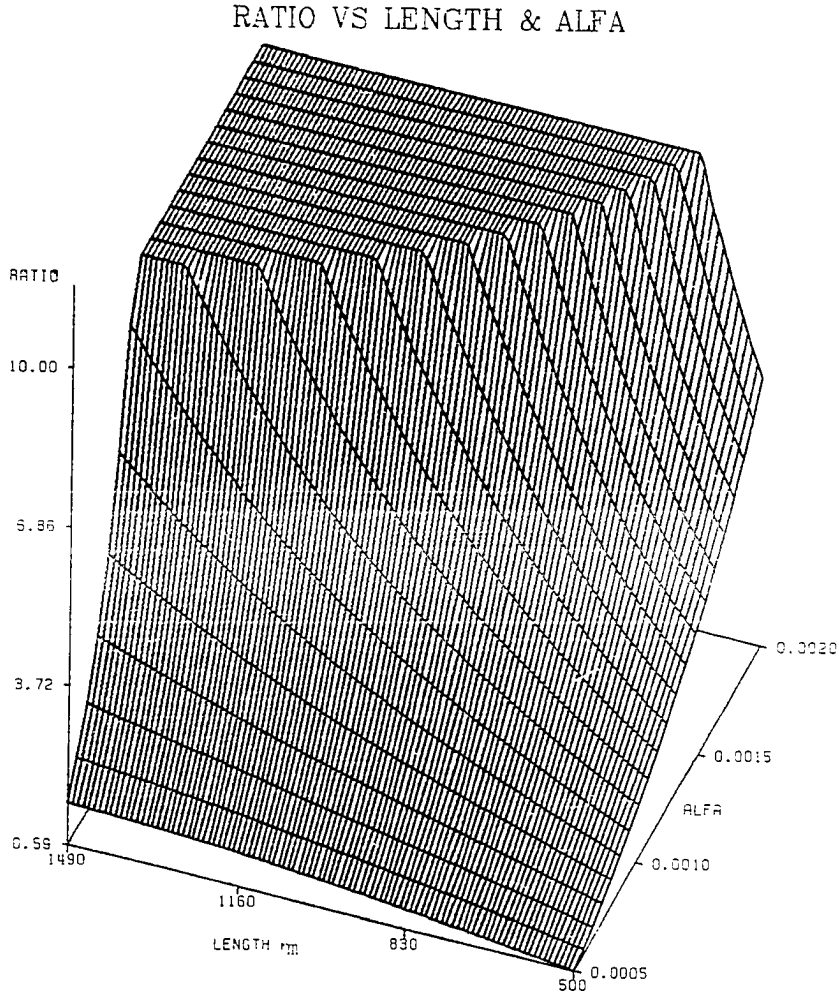

Figure 5.5: RATIO as a function of fiber's length and α.

Modulation frequency=50 kHz
S=0.02
end reflectivity=0.1

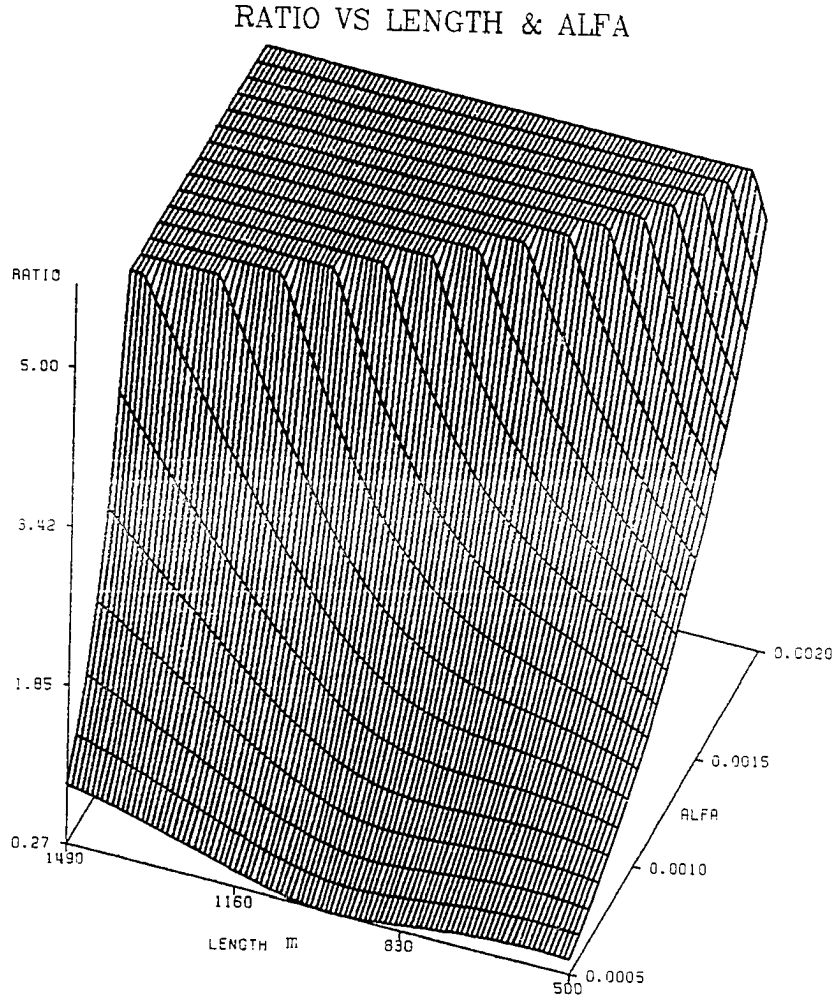

Figure 5.6: RATIO as a function of fiber's length and α

Modulation frequency=0.1 MHz
S=0.02
end reflectivity=0.1

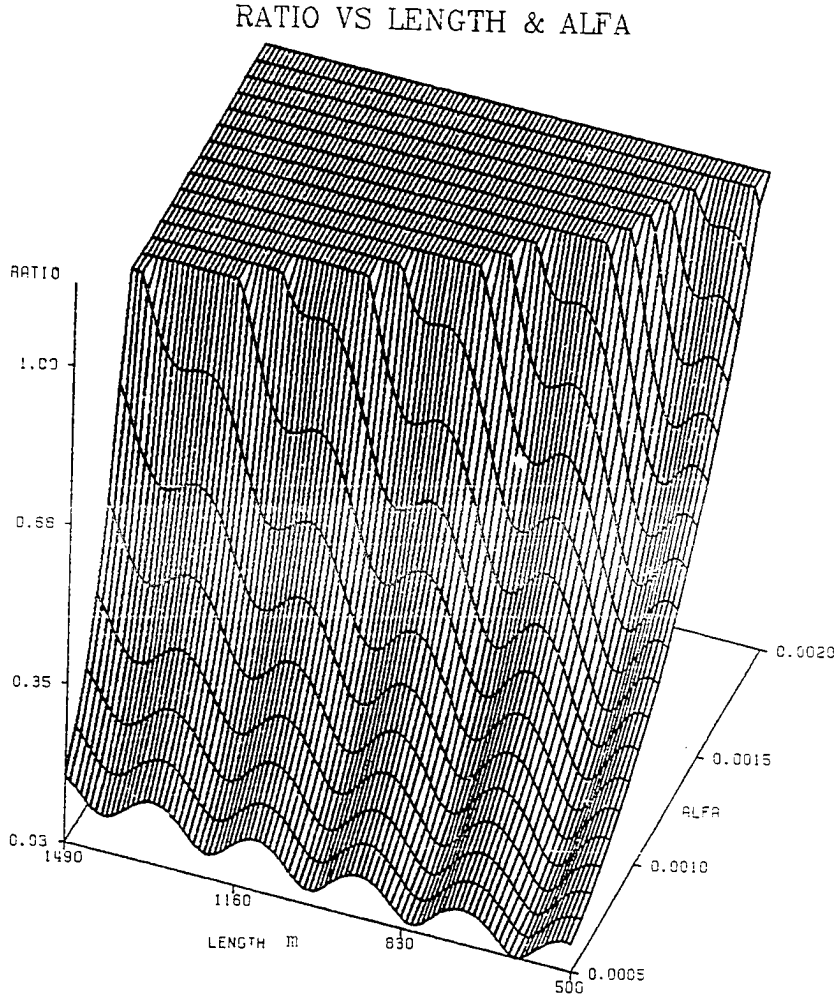

Figure 5.7: RATIO as a function of fiber's length and α.

Modulation frequency=0.5 MHz
S=0.02
end reflectivity=0.1

5.2.2 Effect of S Factor on RATIO

The S factor is the portion of the scattered light guided back towards the transmitter. In section 3.2, an overall review of literature showed that for multimode fibers the S factor is dependent upon the NA and core index of refraction. And for single-mode fibers it is also dependent upon the core radius, normalized frequency, and the spot size. Figures 5.8 through 5.11 show the RATIO as a function of frequency and α. Fibers with S factors of 0.01 and 0.02 and lengths of 500 and 1000 m are chosen. These figures indicate that if all parameters except the S factor for two fibers are the same, the RATIO for the fiber with higher S will be higher than RATIO for fiber with lower S.

5.3 Minimum Frequency for RATIO < 0.1 Condition

When the OFDR technique is used for fault location, or detection of discrete reflections it is very important to cancel the distributed reflections. This process is improved by increasing the lowest value of the modulation frequency. We assume RATIO < 0.1 is low enough to consider that distributed reflections have very small amplitudes when compared with discrete reflections. Frequencies that achieve RATIO=0.1 are plotted as a function of fiber lengths and α in figures 5.12 and 5.13 with respective values of S=0.01 and 0.02.

GRAPH OF RATIO

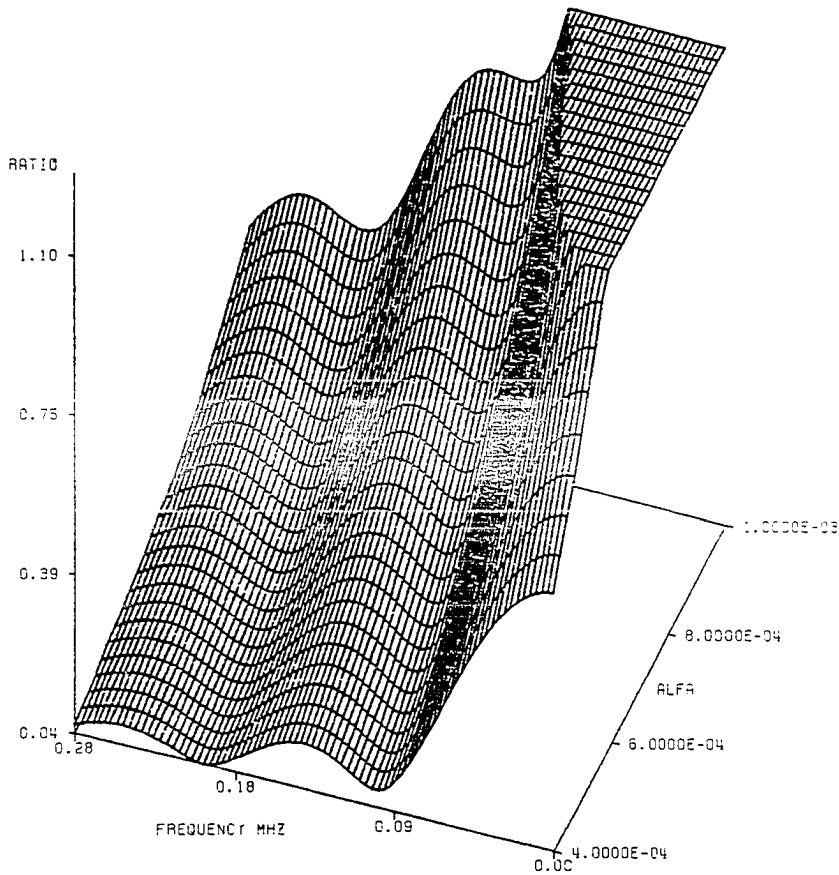

Figure 5.8: RATIO as a function of frequency and α.

Fiber length=500 m
S=0.01
end reflectivity=0.1

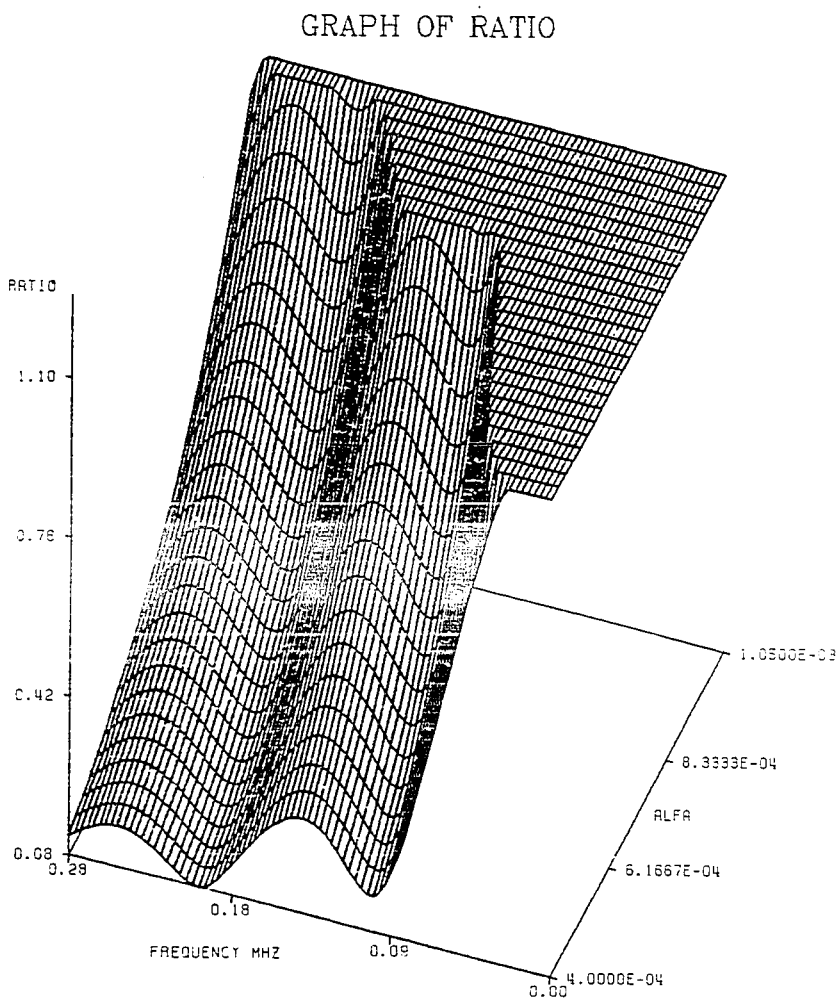

Figure 5.9: RATIO as a function of frequency and α.

fiber length=500 m
S=0.02
end reflectivity=0.1

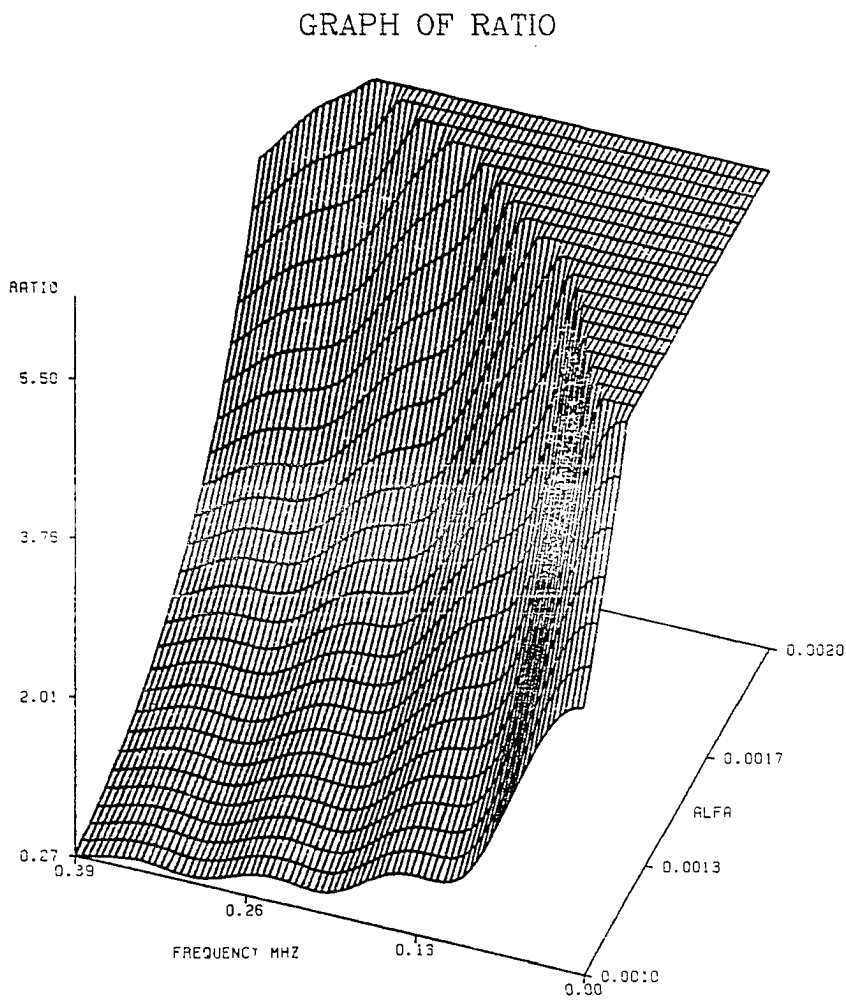

Figure 5.10: RATIO as a function of frequency and α.

Fiber length=1000 m
S=0.01
end reflection=0.1

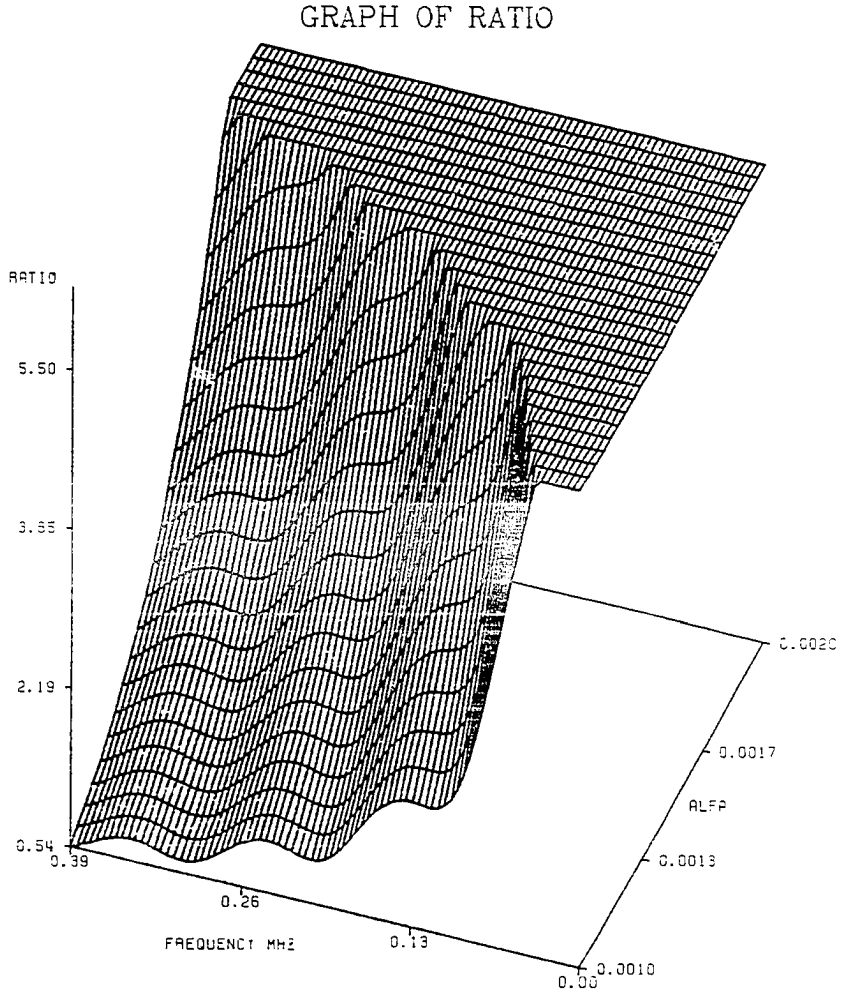

Figure 5.11: RATIO as a function of frequency and α.

Fiber length=1000 m
S=0.02
end reflectivity=0.1

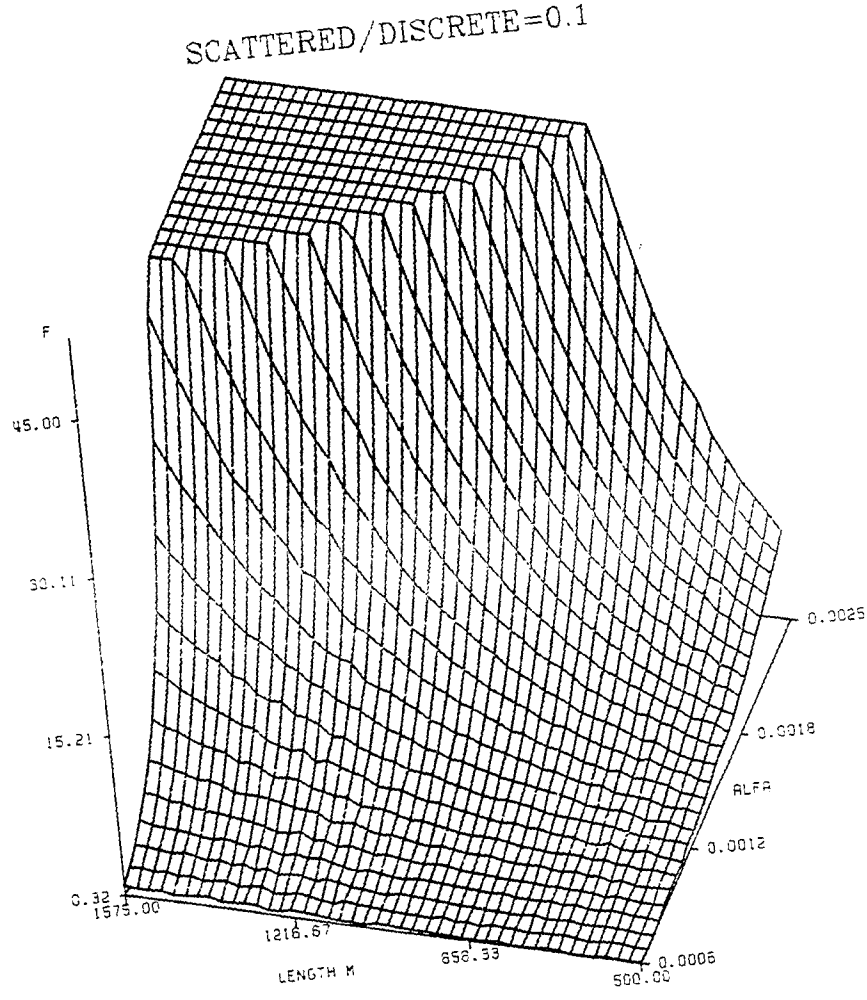

Figure 5.12: Graph of frequencies at which RATIO=0.1 as a function of fiber length.

S=0.01
end reflectivity=0.1

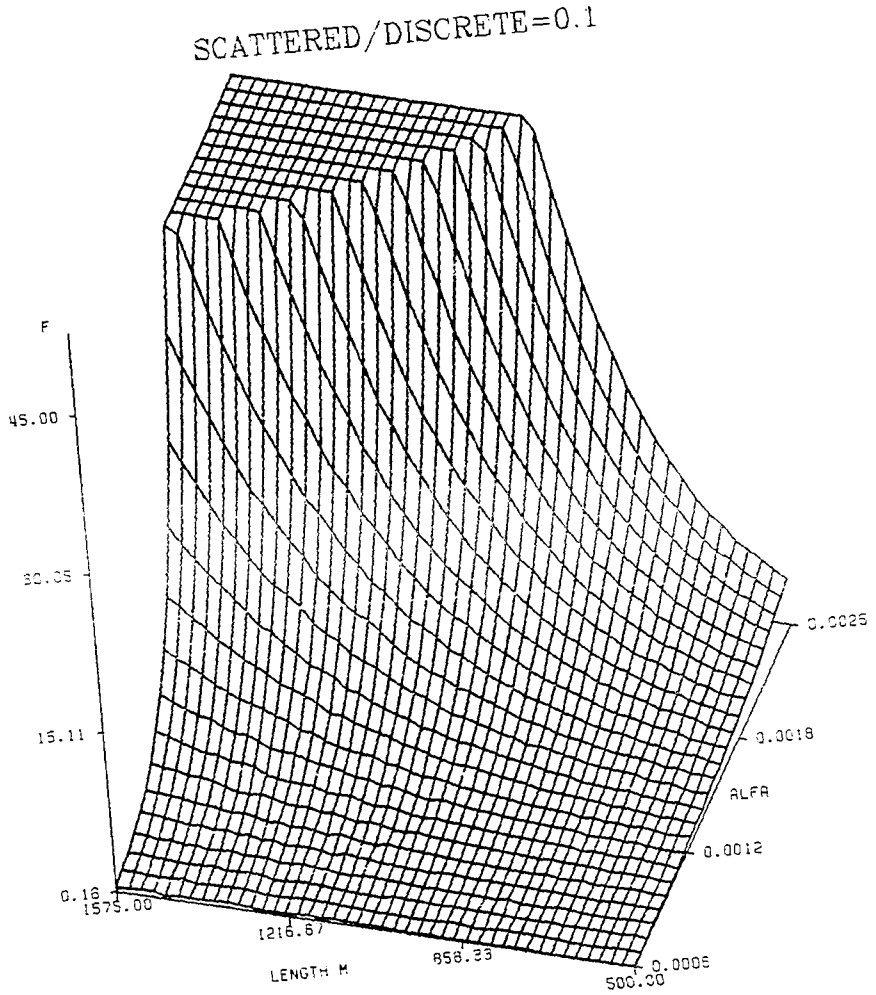

Figure 5.13: Graph of frequencies at which RATIO=0.1 as a function of fiber length and α.

S=0.02
end reflectivity=0.1

CHAPTER VI

MEASUREMENTS

6.1 Technique and Apparatus

The measuring apparatus for this research is shown in figure 6.1. The 2 mW He-Ne laser output passes through an optical polarizer. It is then focused into a KD_2PO_4 electrooptic intensity modulator. The modulation signal is provided by a 0.25 W rf oscillator (0.35-50 MHz). The rf signal is applied to a 2 W tunable power amplifier. Typically the modulator requires 150 V peak-to-peak to provide 15 percent modulation. The modulated beam is focused into the test fiber. Reflected light is directed to the pin diode by means of the beam splitter. The detected signal is amplified and then mixed with the original rf signal by the lock in voltmeter. The phase and amplitude of the reflected signal is proportional to the propagation delay associated with the reflectors, index of refraction, and Rayleigh scattering loss (detailed in chapter 3). Observed reflected power levels are on the order of nanowatts. The lock in voltmeter is particularly suitable for low level applications. Additional problems of rf interference from the high power rf

amplifier, picked up on the lock in voltmeter, are eliminated by carefully shielding the modulator circuitry and the photodiode housing.

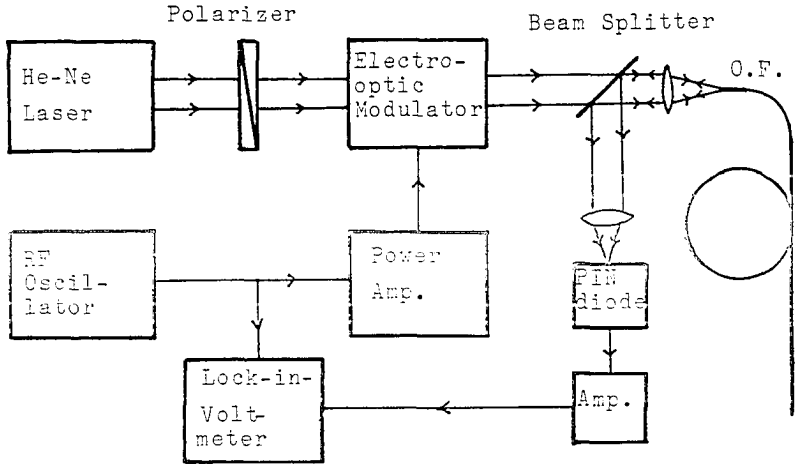

Figure 6.1: Experimental setup

6.2 Testing of the Equipment

The function of each unit in the experimental setup shown in figure 6.1 is tested separately. The following represents the result and importance of each test.

6.2.1 Modulator Linearity Test

The process of intensity modulation of the laser beam is accomplished by biasing the modulator with a fixed retardation to the 50 percent transmission point. This bias is achieved by using a naturally birefringent crystal to introduce retardation of $\pi/2$ to the polarized input beam. Therefore, a small applied voltage modulates the transmitted intensity within the linear part of the modulator characteristics. After biasing the modulator, the test setup shown in figure 6.2 was used to verify the modulation linearity. For the dc modulation voltage varied from 0 to 200 Volts, the modulated beam was recovered by a pin diode and measured by a dc millivoltmeter. Figure 6.3 shows the linearity of the modulator.

6.2.2 Modulation Index Measurement

In order to measure the modulation index, the setup shown in figure 6.4 was used. After biasing the modulator and tuning the rf power amplifier, the rf signal was retrieved by the photodiode, amplified, and observed on the oscilloscope for peak value measurement. The rf signal was then disconnected from the modulator and only the optical carrier

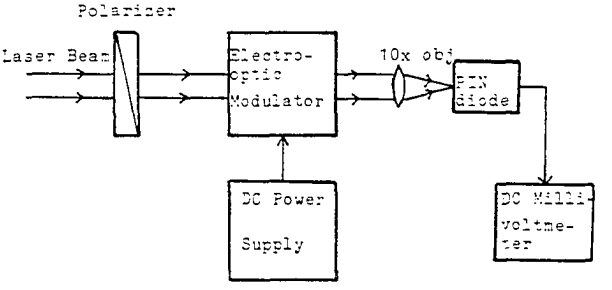

Figure 6.2: Setup for modulator linearity test

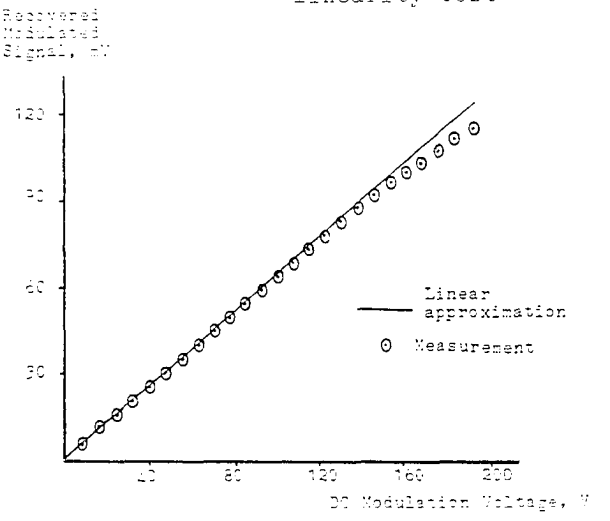

Figure 6.3: Result of modulator linearity test

was detected this time. The modulation index was obtained as

$$m = \frac{\text{optical carrier intensity}}{\text{detected rf amplitude}} \times 100\%$$

Typically 15 percent modulation was obtained, when 150 volts peak-to-peak was applied to the modulator.

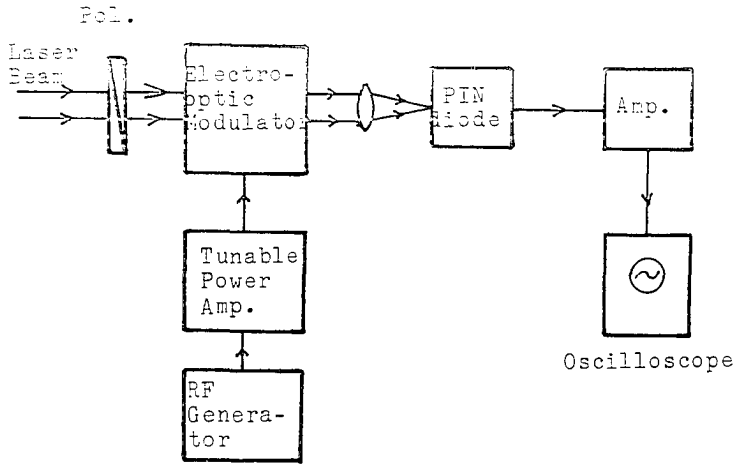

Figure 6.4: Setup for modulation index measurement

6.2.3 dc Reflection Test

In order to investigate the relation between the amplitude of the modulation signal and the amplitude of the reflected signal, the following test was conducted. The test setup is shown in figure 6.5. The modulation signal is provided by a high voltage dc power supply. A 3 m multimode fiber was selected. Score and break technique (S5) was used for fiber end preparation. After biasing the modulator, the modulation voltage (V_{in}) was increased gradually, and reflected signals were detected by means of a pin diode. Figure 6.6 shows the amplitude of the reflected signals vs amplitude of V_{in}. A good linear approximation occurred for V_{in} less than 200 V. Deviation from linearity occurred because of modulator nonlinearity for voltages in excess of 200 V.

6.2.4 Lock In Voltmeter Accuracy Test

The test setup shown in figure 6.7 was used in order to verify the accuracy of the lock in voltmeter. A mirror was placed in the way of the transmitted beam, at an angle of 10^{0} with the plane normal to the propagation axis. Therefore, the reflected light would not interfere with the transmitted beam. After adjusting the modulator and tuning the rf amplifier, the mirror was located in position 1, and reflections were focused on the photodiode. The recovered rf signal was mixed with the attenuated original signal by the lock in voltmeter for phase detection as a reference. The

mirror was then moved back a distance of L. Again, the reflected beam was focused on the photodiode and then applied to the lock in voltmeter. This process was repeated by positioning the mirror at different distances. The result of these measurements is plotted in figure 6.8.

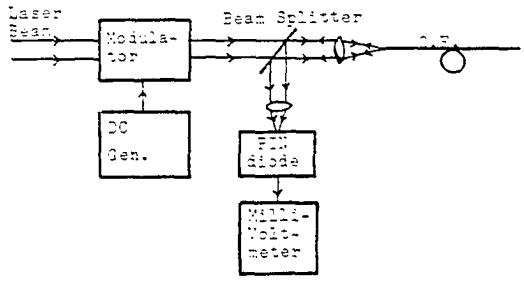

Figure 6.5: Setup for dc reflection test

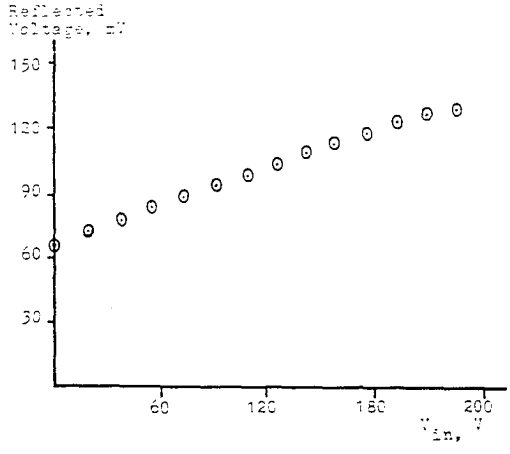

Figure 6.6: Result from dc reflection test

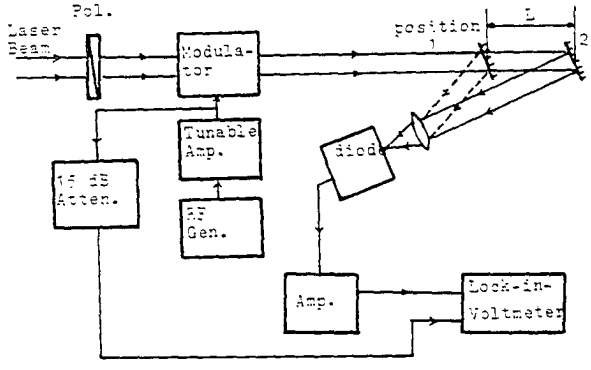

Figure 6.7: Setup for phase measurement of reflections in free space

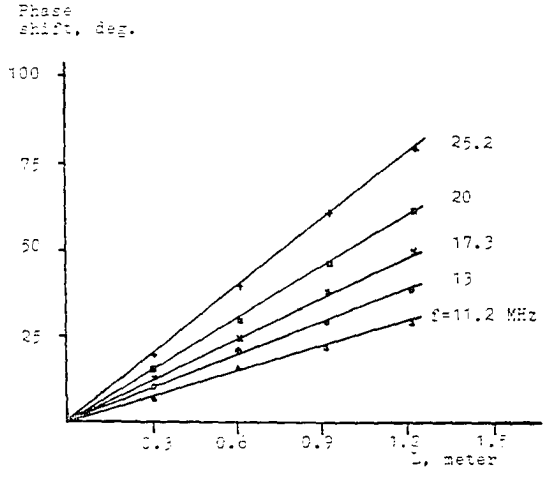

Figure 6.8: Phase delay of reflections in free space for different frequencies

6.3 Phase and Amplitude Measurement of Echos From an Optical Fiber

The setup shown in figure 6.1 was used to observe the phase and amplitude properties of the signal reflected from the optical fiber. The echos from the front face of the fiber were eliminated by cutting the front fiber end at 10^{0}. The modulated beam was launched into the 1 meter length multimode, step index, silica core fiber with an index of refraction n=1.490. The reflected light was directed to the photodiode by the beam splitter. This experiment was performed for two different situations:

(1) No attempt was made to prepare an ideal end cut at the fiber output. Therefore, the Frensnel reflection power fell short of its maximum. A very low level signal was reflected back through the fiber, resulting in a weak signal focused on the photodiode. Figure 6.9 shows the phase and amplitude of the reflected signal for this case.

(2) The fiber end was cut normal to the propagation axis and it was assisted to make end reflections much higher than Rayleigh reflections by using a mirror at the fiber end. In this situation, the level of the reflected signal was high enough to represent a good agreement between predicted and measured values. Figure 6.10 shows the phase and amplitude of the reflected signal.

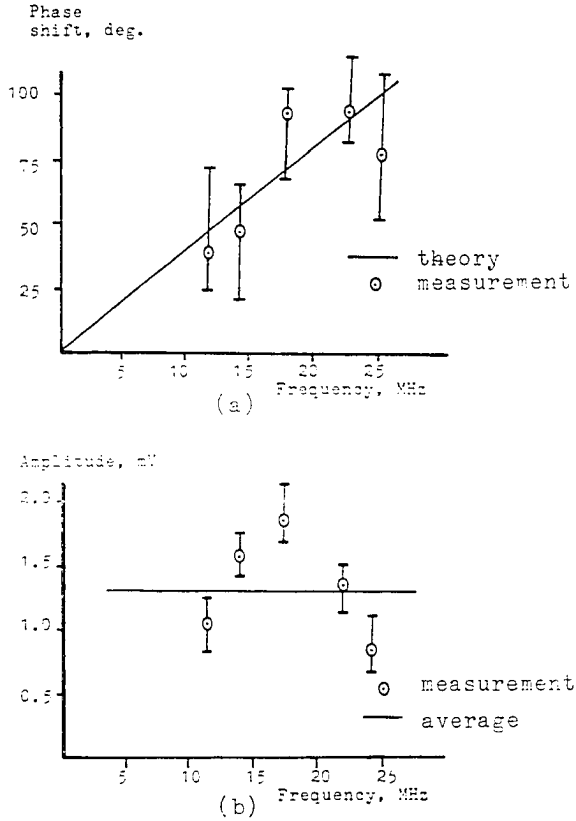

Figure 6.9: Characteristic of the reflections from a 1 m fiber with very low end reflection

(a) phase versus frequency
(b) amplitude versus frequency

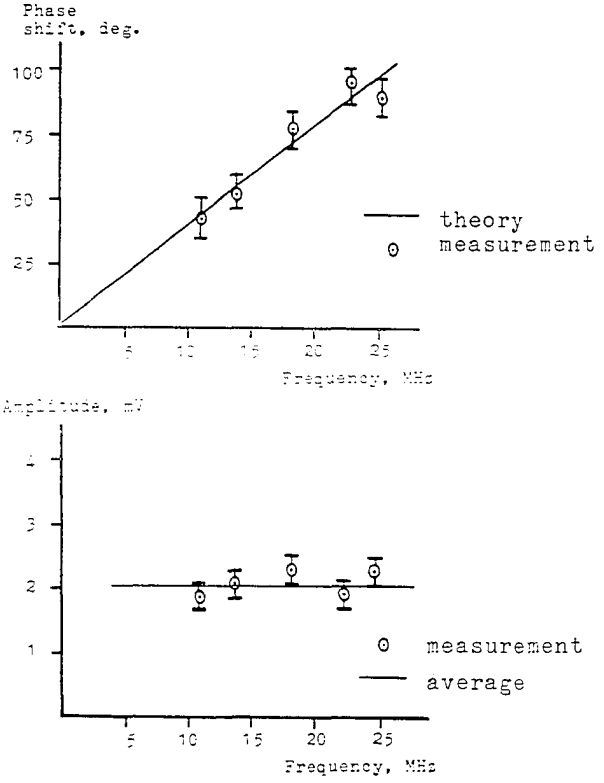

Figure 6.10: Characteristic of the reflections from a 1 m fiber with high end reflections

(a) phase versus frequency
(b) amplitude versus frequency

CHAPTER VII

CONCLUSION

Discrete and distributed reflections in optical fibers have been analyzed by using optical frequency domain reflectometry technique. The technique mentioned here was based on the use of a tunable rf generator output as a modulation signal. Reflectors' positions and properties can be recognised by varying the frequency of modulation and obtaining the phase and amplitude of the reflected signal. The correspondence between phase and frequency is dependent upon the number of reflectors and their relative distances. This technique is capable of detecting reflections from breaks or splices with reflectivity of 1% in fibers with scattering loss more than 10 dB/km. Analysis of the reflected signal when it is contaminated with noise has shown that when SNR at the receiver input is less than 10 dB, breaks or splices with reflectivity of 1% are also detectable.

An alternate OFDR technique would be the application of a constant amplitude rf signal with a periodic linear frequency sweep instead of the single frequency rf signal. This method is much faster than the previous technique

because no extra time for tuning the rf oscillator and analyzing the returned signal is needed. The disadvantage of the sweep technique is the larger bandwidth of the receiver as compared to the single frequency technique. Which of the above techniques is preferable depends on the weakness of the returned signal and the instrumentation that is most easily available. If the returned signal is weak and mixed with noise so that SNR has to be improved by making the receiver bandwidth as small as possible, the use of single frequency technique is wiser. But if narrowing down the receiver's bandwidth doesn't have much effect on the detected signal, the sweep technique would be preferable.

When comparing the time and frequency domain techniques the OFDR technique has shown an improvement of SNR by an average of 40 dB. When discrete and distributed reflections are combined, OFDR will be more efficient for detecting discrete reflections. In time domain technique, however, the positions of the discrete reflectors are directly related to the position of the reflected pulses, therefore, no data analysis is needed.

OFDR technique is not a suitable method for determining Rayleigh reflections, that is, one cannot determine the loss. In other words, distributed reflections can be considered as an infinite number of discrete reflections very close to one another. At high modulation frequencies, the sum of these reflections will approach zero amplitude because of the phase difference interfering to cause near zero amplitude at high

frequencies. Figure 4.10 shows the Rayleigh backscattered signal from a 500 m fiber. The detected signal approaches zero amplitude for modulation frequencies higher than 0.5 MHz.

REFERENCES

(A1) Aoyama, K., Nakagawa, K., and Itoh, T., "Optical Time Domain Reflectometry in a Single Mode Fiber." IEEE J. Quantum Electron., Vol. QE-17, pp. 862-8, June 1981.

(B1) Brinkmeyer, E., "Backscattering in Single Mode Fibers." Electron. Lett., Vol. 16, pp. 329-30, 1980.

(C1) Conduit, A.J., Hullett, J.L., Hartog, A.H., and Payne D.N., "An Optimized Technique for Backscatter Attenuation Measurements in Optical Fibers." Opt. Quantum Electron, Vol. 12, pp. 169-78, 1980.

(G1) Gentile, J., "Characterizing Optical Fibers with an OTDR." Electro Opt. Syst. Design, pp. 47-52, April 1981.

(G2) Gerrard, A., and Burch, J., Introduction to Matrix Methods in Optics., Wiley, 1975.

(H1) Heckman, S., Brinkmeyer, E., and Streckert, J., "Long-Range Backscattering Experiments in Single-Mode Fibers." Opt. Lett., Vol. 6, pp. 634-5, 1981.

(I1) Ippen, E., "Nonlinear Effect in Optical Fibers." in Laser Applications to Optics and Spectroscopy., Addison-Wesley, 1975.

(K1) Kapron, F., Kneller, D., and Garel-Jones, P., in Technical Digest, Third Internationl Conference on Integrated Optics and Optical Fiber Communication (Optical Society of America, Wshington, D.C., 1981), paper WF2.

(K2) Kapron, F., Borrelli, N., and Keck, D., "Birefrigence in Dielectric Optical Waveguides." IEEE J. Quantum Electron., Vol. QE-8, pp. 222-5, 1972.

(L1) Lagakos, N., Bucaro, J., and Jarzynski, J., "Temperature Induced Optical Phase Shifts in Fibers." Appl. Opt., Vol. 20, pp. 2305-8, 1981.

(M1) Mac Donald, R.I., "Frequency Domain Optical Reflectometry." Appl. Opt., Vol. 20, pp. 1840-4, 1981.

(M2) Murakami, Y., Noguchi, K., Ashiya, F., Negishi, Y., and Kojima, N., "Maximum Measurable Distance for a Single-Mode Optical Fiber Fault Locator Using Stimulated Raman Scattering (SRS) Effect." IEEE J. Quantum Electron, Vol. QE-18, pp. 1473-6, 1982.

(M3) Mickelson, A.R. and Eriksurd, M., "Theory of the Backscattering Process in Multimode Optical Fibers." Appl. Opt., Vol. 21, pp. 1898-901, 1982.

(N1) Nakazawa, M., Tanifuji, T., Tokuda, M., and Uchida, N., "Photon Probe Fault Locator for Single-Mode Optical Fiber Using an Acoustooptical Light Deflector." IEEE J. Quantum Electron., Vol. QE-17, pp. 1264-9, 1981.

(N2) Nakazawa, M. and Tokuda, M., "Measurement of the Fiber Loss Spectrum Using Fiber Raman Optical Time Domain Reflectometry." Appl. Opt., Vol. 22, pp. 1910-1983.

(O1) Okada, K., Hashimoto, K., Shibata, T., and Nagaki, Y., "Optical Cable Fault Location Using Correlation Technique." Electron. Lett., Vol. 16, pp. 629-30, 1980.

(P1) Personick, S.D., "Photon Probe-An Optical Fiber Time Domain Reflectometer." Bell Syst. Tech. J., Vol. 56, pp. 355-65, 1977.

(P2) Philen, D., White, I., Kahl, J., and Mettler, S., "Single-Mode Fiber OTDR: Experiment and Theory." IEEE J. Quantum Electron., Vol. QE-18, pp. 1499-1508, 1982.

(R1) Rogers, A.J., "Polarization-Optical Time Domain Reflectometry: A Technique for the Measurement of Field Distribution." Appl. Opt., Vol. 20, pp. 1060-74, 1981.

(R2) Ross, J.N., "Birefringence Measurement in Optical Fibers by Polarization-Optical Time Domain Reflectometry." Appl. Opt., Vol. 21, pp. 2489- , 1982.

(S1) Shibata, N., Tateda, M., Seikai, S.,and Uchida, N., "Measurement of Waveguide Structure Fluctuation in a Multimode Optical Fiber by Backscattering Technique." IEEE J. Quantum Electron., Vol. QE-17, pp. 39-43, 1981.

(S2) Smith, A.M., "Polarization and Magnetooptic Properties of Single-Mode Optical Fibers." Appl. Opt., Vol. 17, pp. 52-6, 1978.

(S3) Smith, A.M., "Birefringence Induced by Bend and Twists in Single-Mode Optical Fibers." Appl. Opt., Vol. 19, pp. 2606-11, 1980.

(S4) Smith, R.G., "Optical Power Handling Capacity of Low Loss Optical Fibers as Determined by Stimulated Raman and Brillouin Scattering." Appl. Opt., Vol. 11, pp. 2489-94, 1972.

(S5) Shadaram, M., Master Thesis, School of Electrical Engineering and Computer Science, University of Oklahoma, 1980.

(U1) Ulrich, R. and Simon, A., "Polarization Optics of Twisted Single-Mode Fibers.", Appl. Opt., Vol. 18, pp. 2241-51, 1979.

(V1) Vit, P. and Rossi, V., "Backscattering Measurements in Optical Fibers: Separation of Power Decays from Imperfection Contribution." Electron. Lett., Vol. 15, pp. 467-9, 1979.

(Y1) Yariv, A., Introduction to Optical Electronics, Holt, Rinehart and Winston, pp. 320-8, 1976.

APPENDIX

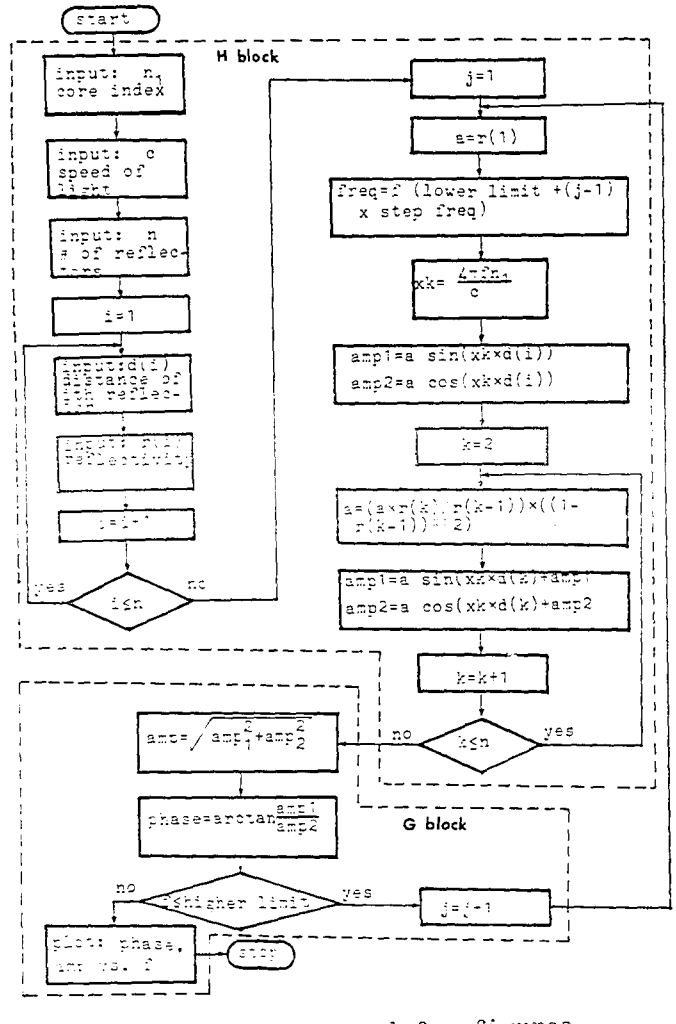

Figure A.1: Algorithm used for figures 4.1 through 4.8

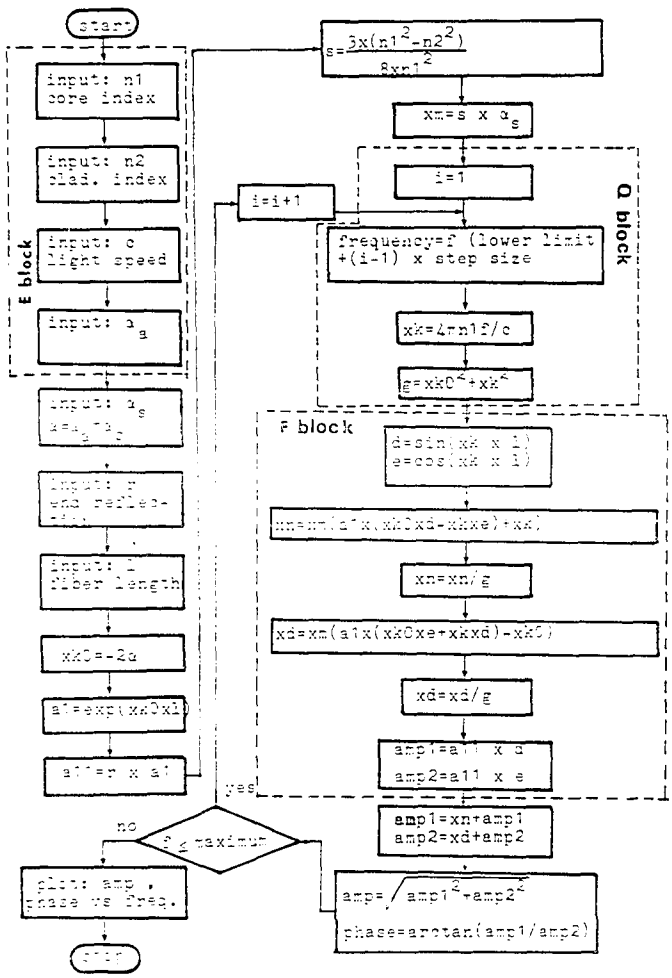

Figure A.2: Algorithm used for figures 4.9 through 4.13

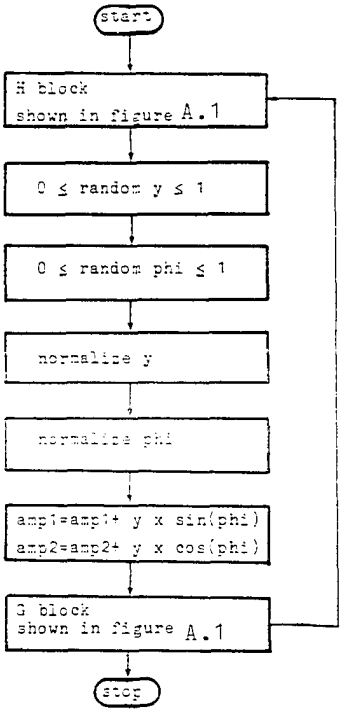

Figure A.3: Algorithm used for figures 4.18 and 4.19

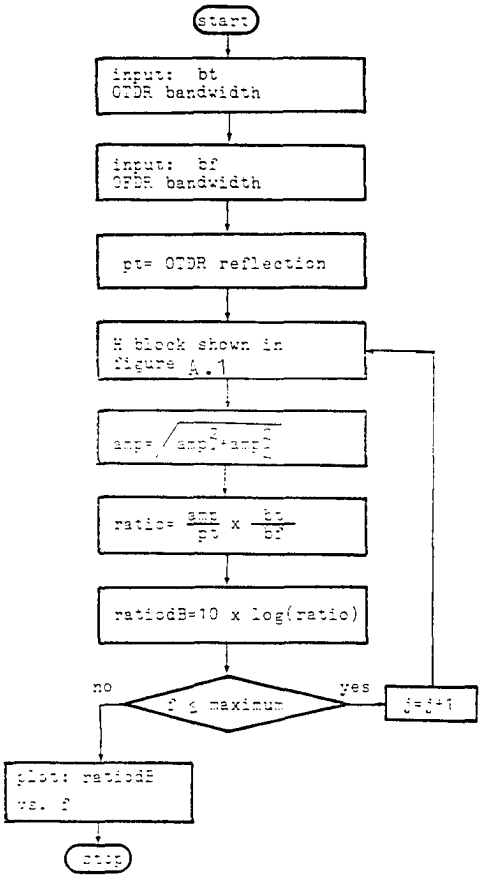

Figure A.4: Algorithm used for figures 4.22, 4.23, and 4.24

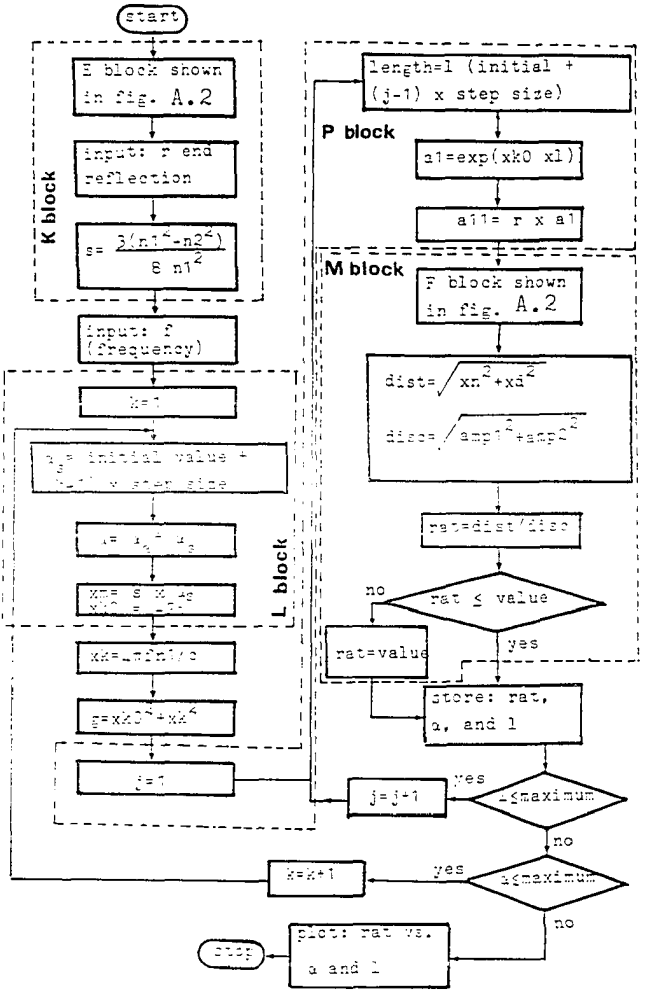

Figure A.5: Algorithm used for figures 5.5, 5.6 and 5.7

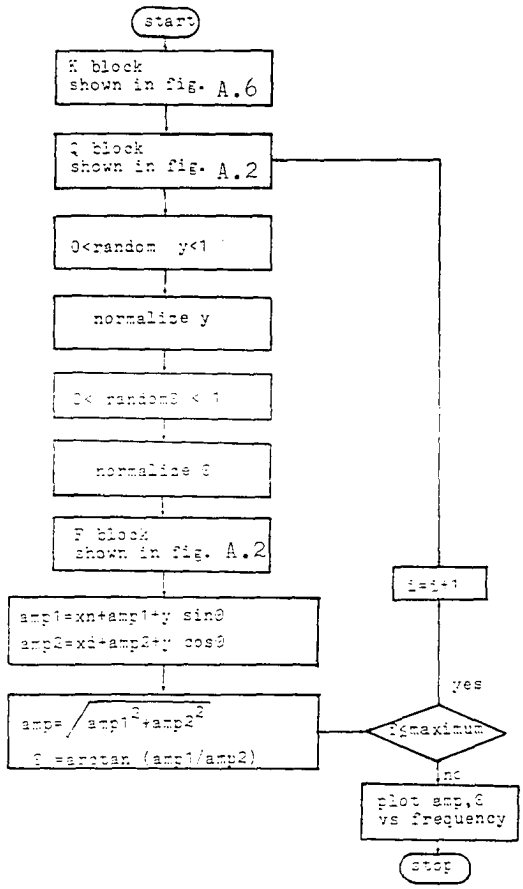

Figure A.6: Algorithm used for figures 4.20 and 4.21

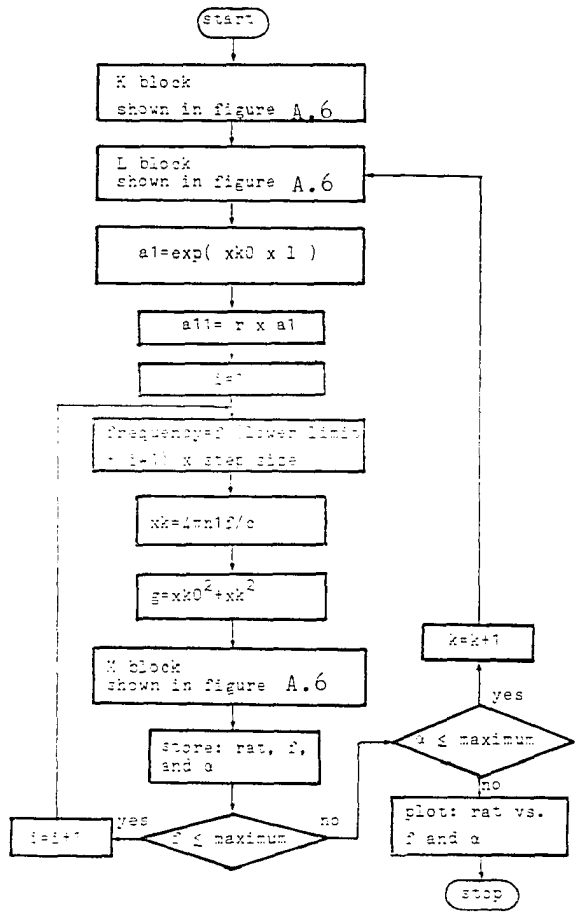

Figure A.7: Algorithm used for figures 5.8, 5.9, 5.10, and 5.11

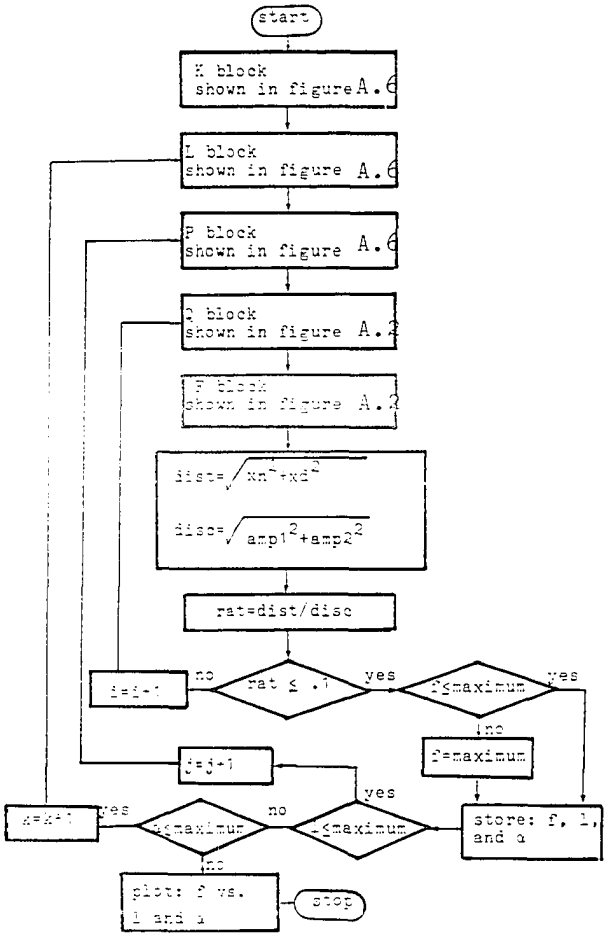

Figure A.8: Algorithm used for figures 5.12 5.13